A.Dian Permana-5_Usulan.pdf

by

Submission date: 09-Dec-2022 07:59AM (UTC+0700)
Submission ID: 1975829991
File name: A.Dian Permana-5_Usulan.pdf (2.69M)
Word count: 13513
Character count: 68344

143 (2022) 213175

Contents lists available at ScienceDirect

Biomaterials Advances

journal homepage: www.journals.elsevier.com/materials-science-and-engineering-c

Development of chloramphenicol wound dressing protein-based microparticles in chitosan hydrogel system for improved effectiveness of dermal wound therapy

Tri Puspita Roska, Sartini, Mukarram Mudjahid, Ardiyah Nurul Fitri Marzaman, Nana Novriana Payung Datu, Andi Dian Permana *

Faculty of Pharmacy, Hasanuddin University, Makassar 90245, Indonesia

ARTICLE INFO

Keywords:
Chloramphenicol
Hydrogel
Microparticle
Skin wounds
Whey protein

ABSTRACT

Skin wounds have been reported to increase the number of microbial colonies susceptible to infection. Treatments using oral antibiotics have been limited due to their toxicity and hydrophobic characteristics. In this study, we developed a formulation of chloramphenicol microparticles (CPL MPs), which was modified into chitosan hydrogel to increase treatment efficiency in targeting infections and creating an optimal environment to support the healing process. CPL MPs were prepared by a cross-linker stabilized method using whey protein (WPI) biopolymer, and the CPL MPs hydrogel was designed using chitosan biopolymer. Based on the result, CPL-loaded MPs showed desired physical and encapsulation characteristics. In the *in vitro* study, drug release of CPL MPs in simulated wound fluid represented approximately 90.00 ± 7.01 % of the system after 24 h. The antibacterial activity of CPL-loaded MPs formulation (MIC value 12.5 μg/mL, MBC 25 μg/mL) was effective as MIC concentration increased. Furthermore, the formulation of CPL MPs to hydrogel showed a better dermatokinetic profile compared to hydrogel with pure CPL. Interestingly, the antibacterial activity of the *ex vivo* infection model showed that *Staphylococcus aureus* activity decreased by up to 99.98 % after 24 h administration of CPL MPs hydrogel when compared to pure-CPL hydrogel and blank hydrogel. These studies have confirmed that incorporating CPL MPs into hydrogel can provide a promising approach to skin infection treatment.

1. Introduction

A skin wound is a condition in which the skin has impaired integrity, anatomical structure and tissue function, and may be caused by chronic disease, burns or postoperative trauma. Skin wounds are a healthcare problem that is estimated to occur in about 4–5 % of the adult population [1]. Injuries that compromise the skin's integrity allow microorganisms to colonize the area. This can lead to infection issues that can extend a patient's treatment time and necessitate the administration of more medication. The most common aerobic microorganisms causing wound infections include *S. aureus*, *S. pyogenes*, *P. aeruginosa*, MRSA, *S. epidermidis*, *Enterococcus faecalis*, coliforms, and *Acinetobacter baumannii* [2]. Wound infections can cause bacteremia, sepsis, and organ dysfunction, so an effective method is needed to prevent wound infections, one of which is the administration of appropriate topical antibiotics [3].

One antimicrobial with a broad spectrum of action is chloramphenicol (CPL), which is used for skin infections and can maintain its activity against bacterial resistance, with a bacteriostatic mechanism specifically inhibiting bacterial protein synthesis [4]. However, the effectivity of oral route of CPL is still limited due to its toxicity [5], and the physicochemical properties of hydrophobicity, make it difficult to penetrate the skin and inhibit drug transport to the target of infection [6]. This limitation can be overcome *via* the dermal route, which facilitates the loading of hydrophobic drugs with direct action activity to the target of infection.

Drug delivery systems targeting local infections could be developed by designing drugs into microparticles [7]. Microparticles (MPs) are widely preferred because they responsively release drugs, increase the effectiveness of the drug on the target, and provide local effects on the skin. In addition, drug-containing MPs offer high drug-loading flexibility and good physical and chemical stability [8]. MPs have also been reported to be designed for local administration with desired effects, including wound care. The MPs approach has also been widely

* Corresponding author at: Faculty of Pharmacy, Hasanuddin University, Indonesia.
E-mail address: andi.dian.permana@farmasi.unhas.ac.id (A.D. Permana).

https://doi.org/10.1016/j.bioadv.2022.213175
Received 15 September 2022; Received in revised form 15 October 2022; Accepted 26 October 2022
Available online 1 November 2022

developed for the treatment of infectious diseases to increase efficiency at selectively targeting infections through specific stimulus responses [9].

The drug substance can be incorporated into MPs through various methods such as ionotropic gelation, single or double emulsification, polymerization, and stabilization with cross-linkers [10]. MPs prepared by a cross-linker method using natural biopolymers as drug carriers offer optimal drug loading. Hydrophobic drug encapsulation using natural biopolymers was chosen because of its biodegradability, biocompatible, and suitability for skin delivery system formulation [11]. Whey protein is a high-quality protein from cheese processing or cow's milk and is primarily consisted of major proteins including β-lactoglobulin, α-lactalbumin, immunoglobulin, and lactoferrin [12]. A study has shown that the binding of whey protein biopolymers with hydrophobic drugs can increase drug solubility and dissolution [13]. Liu et al. used whey protein for curcumin encapsulation by employing the spray-drying method to increase curcumin solubility and bioavailability [14]. This can be chosen as a strategy to increase the effectiveness of drugs in treating skin infections. However, there are limitations in using whey protein in formulations because it tends to have a weak protein bond, is easily damaged by heating, and may be susceptible to degradation. Therefore, hydrogel formulation is one of the preparations to overcome this problem.

Hydrogels are polymer networks with hydrophilic properties, which are needed in wound treatment because they have excellent biocompatibility and provide an optimal environment for wound healing. Hydrogels can be applied in various physical forms, such as nanoparticles, MPs, and films [15]. Chitosan, the natural polymers in the manufacture of hydrogels, contain many hydroxyl and amine groups typically used as functional groups to react with cross-linking agents, which stabilize the protein structure [16]. In the treatment of wound infections, there are several reported benefits of using chitosan as a biopolymer, including good antibacterial activity [17], anti-inflammatory and hemostatic properties, enhanced skin regeneration; superior biocompatibility and biodegradability; good water absorption and skin occlusivity properties; and due to the presence of amino and hydroxyl groups in the molecular chain, many biological activities can be improved by grafting on additional groups and chemical elements [17,18].

For the potential enhancement of wound infection therapy, in this study, we provide a novel combination delivery method of chitosan hydrogel and chloramphenicol microparticles (CPL MPs). CPL MPs was formed and optimized by solvent evaporation and stabilized using a cross-linker. Additionally, tests were done on drug loading, entrapment effectiveness, zeta potential, particle size, polydispersity index, and antibacterial activity. The fabrication capacity to deliver CPL intradermally was further tested in an *ex vivo* dermatokinetic study on healthy rat skin. Lastly, the penetration and antibacterial activity of the formulation were evaluated in an *ex vivo* skin infection model. The major findings of this study have the potential to provide new insights for solving problems in the treatment of skin wound infections.

2. Materials and methods

2.1. Materials

Whey protein (WPI) containing 80 % was gifted by Glanbia Nutritionals, Inc., Fitchburg, USA. Chloramphenicol, Chitosan (MW 161.156 and deacetylation degree ≥ 75 %), glutaraldehyde, 2-alpha naphthol, tryptone soya agar (TSA) medium, nutrient broth (NB) medium, phosphate-buffered saline (PBS), and sodium hydroxide were purchased from Sigma–Aldrich Pte Ltd., Singapore, Singapore. The reagents utilized in this investigation were all analytical grade.

2.2. Preparation of CPL MPs

CPL MPs were prepared according to a previous study [19], with slight modifications. WPI (with concentration of 2.5 %, 5 %, 10 %, 15 % and 20 % (w/v)) was dispersed in deionized water, and the protein solution's pH was adjusted to 8 using NaOH (1 M). The solution was swirled for 1 h with a magnetic stirrer before being refrigerated overnight (4 °C) to fully hydrate the biopolymer. The solution was centrifuged at 1000 rpm for 5 min, and the supernatant was separated for further use. CPL (with a concentration of 12.5, 25, 50, 100, and 200 mg/mL) was dissolved in 5 mL ethanol and added to 20 mL of protein solution dropwise while continuously stirring at a temperature of 40 °C. Immediately after dissolution using methanol, 2 ml of 5 % (v/v) glutaraldehyde was added to facilitate cross-linking of the MPs. The detailed concentration of formulation is depicted in Table 1. The cross-linking procedure was carried out for 24 h at 40 °C with agitation; this also caused any residual organic solvent to evaporate. The obtained dispersion was thoroughly washed with deionized water three times. The mixtures were then freeze-dried.

2.3. Characterization of CPL MPs

2.3.1. Evaluation of particle size, zeta potential and polydispersity index (PDI)

The particle size, polydispersity index (PDI) and zeta potential of formulation were determined using the size analyzer (Malvern

Table 1
Details of the different formulation characteristics utilized to create CPL MPs, including their PDI, zeta potential, and particle size (means ± SD, $n = 3$).

Formulation code	WPI in water (%)	CPL in ethanol (mg)	Ratio WPL: CPL	Particle size (μm)	PDI	Zeta potential (mV)
MP1	5	12.5	4:1	1.33 ± 0.09	0.127 ± 0.005	−28.27 ± 0.81
MP2	5	25	4:1	1.40 ± 0.14	0.129 ± 0.005	−29.25 ± 1.01
MP3	5	50	4:1	1.44 ± 0.05	0.13 ± 0.003	−29.44 ± 0.67
MP4	5	100	4:1	1.45 ± 0.11	0.14 ± 0.007	−29.14 ± 1.06
MP5	5	200	4:1	1.47 ± 0.10	0.13 ± 0.010	−29.21 ± 1.65
WP1	2.5	50	4:1	0.56 ± 0.13	0.13 ± 0.004	−24.67 ± 0.71
WP2	10	50	4:1	2.92 ± 0.20	0.13 ± 0.005	−31.95 ± 0.87
WP3	15	50	4:1	7.65 ± 0.99	0.14 ± 0.005	−34.23 ± 1.14
WP4	20	50	4:1	11.42 ± 1.07	0.14 ± 0.009	−35.17 ± 0.84
CP1	10	50	1:1	134.62 ± 10.29	0.63 ± 0.029	−27.73 ± 1.43
CP2	10	50	2:1	33.03 ± 4.08	0.40 ± 0.006	−28.36 ± 0.91
CP3	10	50	8:1	1.29 ± 0.05	0.13 ± 0.007	−32.32 ± 2.00
CP4	10	50	16:1	1.29 ± 0.07	0.12 ± 0.009	−32.56 ± 2.04

Instruments, Malvern, UK). The MPs were first dispersed with deionized water (0.01 % v/v), and 1 ml of each sample was used for the analysis process. All samples were analyzed at 25 °C and a scattering angle of 90°.

2.3.2. Measurement of entrapment efficiency (EE) and drug loading (DL) percentages

Microparticle EE was measured using the indirect method. CPL MPs suspension was centrifuged at 11 rpm for 20 min to separate the supernatant. The supernatant was then analyzed using a UV–Vis spectrophotometer at a wavelength of 488.7 nm after being derivatized with 2-alpha naphthol (0.01 M) and sodium bicarbonate (0.01 M). A derivatization procedure was performed on CPL to produce peaks that did not overlap with WPI and showed accurate measurement data. The reduced CPL MPs solution was created by dissolving the CPL MPs in methanol, then reacting it with zinc powder and HCl (12 M) while stirring it for 5 min in bath water at a temperature of 50 °C. The reduced solution was filtered into a flask and diluted with deionized water. In a volumetric flask containing the CPL MPs solution, 1 mL of 2-alpha naphthol and 0.5 mL of sodium bicarbonate (0.1 M) were added to complete the reduced process. To create an orange-red result, the solution was heated at 70 °C in bath water for 10 min. The amount of CPL was calculated according to the standard curve equation $Y = 0.0769x - 0.0097$. The encapsulation efficiency of CPL MPs (EE) % is the actual amount of the CPL found in MPs divided by the total amount of the CPL added during the preparation. Drug loading of CPL (DL) % is the mass of the CPL-MPs in the dried powder divided by the total mass of the MPs recovered from the drying process. The calculation of % EE and DL follows the equations below [20]:

$$\%\text{Entrapment Efficiency (EE)} = \frac{\textit{Total drug amount} - \textit{unencapsulated drug amount}}{\textit{total drug amount}} \times 100\% \quad (1)$$

$$\%\text{Drug Loading (DL)} = \frac{\textit{Mass of encapsulated drug}}{\textit{total mass of microparticle}} \times 100\% \quad (2)$$

2.3.3. Powder X-ray diffraction (PXRD) analysis

The crystallinity pattern of the sample was analyzed with a powder X-ray diffraction (Rigaku Corporation, Kent, England) instrument using 1 g of sample in a very high-resolution Cu-K_α radiation diffraction system. The CPL MPs was placed in an aluminum holder at a voltage of 40 kV, current of 30 mA and scanned 2θ angle range of 10 to 90°.

2.3.4. Differential scanning calorimetry (DSC) analysis

The materials were thermally examined using a DSC 2920 TA instrument (Surrey, UK). The detection parameters for this measurement were a 5 mg powder sample, a temperature range of 25° to 300 °C, a heating rate of 10 °C/min, and a nitrogen cleaning rate of 50 ml/min.

2.3.5. Fourier-transform infrared spectroscopy (FT-IR) analysis

Chemical interaction between chemical components in CPL MPs in WPI polymer was analyzed by FT-IR spectrophotometer instrument (Accutrac FT/IR-4100™ Series, Perkin Elmer, USA) in the wavenumbers range of 4000–400 cm^{-1}.

2.3.6. Scanning electron microscope analysis

A scanning electron microscope (TM3030 microscope, Hitachi, Krefeld, Germany) was used to examine the morphologies of CPL MPs. CPL MPs were freeze-dried under vacuum by lyophilizing. The CPL MPs were directly attached to the carbon tape and observed with the following operating conditions: accelerating voltage 15 kV, probe current 45 nA, and counting time 60 s.

2.3.7. In vitro release studies of CPL MPs

In vitro drug release of CPL MPs and CPL using simulated wound fluid. Simulated wound fluid was prepared using 0.36 g of sodium hydrogen carbonate, 5.84 g of sodium chloride, 0.28 g of calcium chloride, 30.30 g of potassium chloride, and 33.00 g of bovine albumin in 1000 mL of deionized water [21]. Two Erlenmeyers contained 50 mL of simulated wound fluid for each formulation. CPL MPs equivalent to 50 mg of CPL were added into simulated wound fluid with 5 mL of samples taken at predetermined time intervals (0.25 h, 0.5 h, 1 h, 2 h, 3 h, 4 h, 5 h, 6 h, 7 h, 8 h and 24 h) and replaced with the same volume of new release media. The test was carried out at a temperature of 37 °C and a speed of 100 rpm. The CPL released was further determined using a UV-Vis spectrophotometer. The amount of CPL in simulated wound fluid was calculated according to the standard curve equation $Y = 0.0368x + 0.011$ with $R^2 = 0.9996$ and the drug release percentage was calculated using the equation below [22]:

$$\%\text{Drug released} = \frac{\textit{Amount of CPL release}}{\textit{Amount of CPL tested (50 mg)}} \times 100\% \quad (3)$$

2.3.8. Mathematical modeling of the kinetics of drug release

The principal mathematical models of drug release were tested, along with the relevant equations and parameters, using the Excel® (Microsoft Corporation, Redmond, USA) Add-in-DDSolver to model the systems' drug release data. The adjustment of the theoretical models to the experimental data was compared using the adjusted coefficient of determination (adjusted-R^2). The kinetics model follows the equations below [23]:

Zero-order:

$$Q_t = Q_0 + K_0 t \quad (4)$$

First-order:

$$\ln Q_t = \ln Q_t + K_1 t \quad (5)$$

Higuchi:

$$Q_t = K_H \sqrt{t} \quad (6)$$

Hixson–Crowell:

$$Q_0^{1/3} - Q_t^{1/3} = K_s t \quad (7)$$

Korsmeyer–Peppas:

$$Q_t = K_n t^n \quad (8)$$

where Q_0 is the preliminary value of Q_t, t is the time, n is the exponent of diffusion release, K_0, K_1, K_H, K_n, and K_s are the coefficients of release according to the relevant kinetic model, and Q_t (%) is the percentage of CPL released at time t.

2.4. In vitro antibacterial activity of CPL MPs

2.4.1. Preparation of bacterial cultures

The bacterial strain used was *Staphylococcus aureus* (ATCC®25923), which was stored at 4 °C and sub-cultured in fresh media. Bacterial culture was prepared by growing bacteria on TSB media with a

temperature of 37 °C. Test bacteria are made equivalent to 0.5 McFarland equivalent to 2 × 10^8 CFU/mL.

2.4.2. Minimum inhibitory concentration (MIC) and minimum bactericidal concentration (MBC) evaluation

The MIC and MBC from CPL and CPL MPs were determined using microtiter dilution techniques in accordance with the Clinical and Laboratory Standards Institute protocol [24]. CPL and CPL MPs solution with a concentration of 1000 µg/mL was made in a 10 mL volumetric flask. The sample was entered into 96-well plates with a concentration of 100 µg/mL. Next, 100 µL of bacterial suspension was added to the wells, then homogenized using micropipettes. TSB with a concentration of 100 µl medium was added to the wells. Wells containing only pure CPL and TSB media alone were used as the positive and negative control, respectively. All filled wells were closed and incubated at 37 °C for 24 h. To determine MBC value, 20 µL from 96-well plates with selected MIC was cultured on a Petri dish containing TSA medium and incubated at 37 °C for 24 h. After that, the number of bacteria in the Petri dish colony was then determined. MBC was defined as the lowest concentration that eliminates 99.9 % of bacterial growth.

2.4.3. Time–kill assay of CPL MPs

Time–kill assay of CPL and CPL MPs against *Staphylococcus aureus* (SA) was determined. CPL, blank MPs, and CPL MPs were added to the bacterial solution in the same quantities as MIC, 2 × MIC, and 4 × MIC, resulting in 2 × 10^5 CFU/mL of bacteria. After that, bacterial cultures were cultured at 37 °C. 20 µL aliquot from the culture was collected at specified time intervals and inoculated aseptically into a Petri dish containing TSA medium. The Petri dish was then incubated at 37 °C for 24 h. The procedure was performed with 3 replications and created a log CFU/mL curve against time. CPL, blank MPs, and CPL MPs were added to the bacterial solution in the same quantities as MIC, 2 × MIC, and 4 × MIC, resulting in 2 × 10^5 CFU/mL of bacteria.

2.4.4. Evaluation of hemolytic activity

By incubating the sample with red blood cells (RBC) and quantifying the percentage of hemoglobin produced from lysed erythrocytes, the overall hemolysis of the formulation was examined. *In vitro* hemolytic assays were carried out in accordance with a previously described method to determine the hemolytic activity of CPL, CPL MPs and CPL MPs hydrogel [25]. First, EDTA tubes containing freshly drawn rat blood were centrifuged for 10 min at 3000 rpm to separate the RBCs. After scraping off the plasma layer at the top of the tube, the remaining cells were further washed twice with PBS and diluted to 1:10, v/v. We mixed 100 µL of the prepared cell suspension with 900 µL of the sample containing CPL, CPL MPs and CPL MPs hydrogel (serially dissolved in PBS) at concentrations ranging from 5 to 500 mg/L. After 60 min of incubation at 37 °C, the mixture was centrifuged at 3000 rpm for 10 min. Free hemoglobin was estimated using UV–visible spectroscopy measurements by analyzing the supernatant taken at wavelength 540 nm. Minimal (negative) and maximum (positive) hemolytic controls were performed using phosphate-buffered saline and distilled water, respectively. Blood sample hemolysis was analyzed by visually inspecting the colour changes in the serum and plasma. For each concentration, the experiments were repeated three times. In the following equation, we included the hemolysis percentage calculation:

$$\text{Hemolysis}\ (\%) : \frac{test\ sample - negative\ control \times 100}{positive\ control - negative\ control} \tag{9}$$

2.5. Formulation of chitosan hydrogel from CPL MPs

Chitosan was dissolved in 2 % acetic acid solution at 60 °C to produce the CPL MPs hydrogel. The chitosan solution was combined with glycerin (10 % w/w) and DMDM hydantoin (0.01 % w/w) while being stirred with a magnetic stirrer. CPL MPs (1 % w/w) were then added to the mixture. The foaming components of the preparation were eliminated using a sonicator for 30 min at a temperature of 50 °C, thereby adjusting the hydrogel pH to 5 with the addition of NaOH 8.3 M. As a control, a hydrogel containing CPL was created.

2.6. Characterization of CPL MPs hydrogel

2.6.1. pH measurement

A pH meter was used to determine the pH of CPL MPs hydrogel by inserting the electrode into the gel and recording the result after 2 min. All measurements are carried out 3 times to obtain the average value and standard deviation.

2.6.2. Evaluation of viscosity and rheology

With the use of a Brookfield viscometer with a seven-speed spindle running at 50 rpm, the viscosity of the CPL hydrogel was measured. The rheology of the CPL hydrogel was also determined using the same seven-speed spindle tool. Measurements are carried out at speeds of 5, 10, 20, 50, and 100 rpm.

2.6.3. Spreadability

Two sets of standard-sized glass slides were taken in this study. The spreadability of the hydrogel was evaluated by applying 0.5 g of the gel to a circle that had been previously marked on a glass plate with a diameter of 2 cm and then again using a second glass plate. After 1 min, the diameter of the hydrogel was measured. The spreadability measurement was carried out with loads of 500 g.

2.6.4. Skin occlusivity examination

The previous technique was used to test *in vitro* skin occlusivity [26]. The 100 mL beaker was filled with 50 mL of deionized water, which was covered carefully with Whatman filter paper. Whatman filter paper with a size of 2.5 mm was applied with 250 mg of hydrogel. As a control, filter paper without CPL MPs hydrogel was used. All samples were stored at a temperature of 32 °C, and the weight of Whatman paper was calculated at 0 h, 6 h, 24 h and 48 h. Occlusivity (O) was calculated through Eq:

$$\text{Occlusivity percentage}\ (\text{O}) = \frac{mass\ of\ control - mass\ of\ sample}{mass\ of\ control} \times 100\% \tag{10}$$

2.6.5. Extrudability percentage

About 10 g of hydrogel were sealed inside a collapsible aluminum tube, the end of which was crimped, and a clamp was used to keep the tube from unwinding. The gel was released after the cap was removed, and the quantity of gel that was extruded was measured. The amount of gel that was forced out of the extruder was determined as follows:

$$\%\text{Extrudability} : \frac{total\ mass\ of\ extruded\ hydrogel}{Total\ mass\ of\ hydrogel} \times 100\% \tag{11}$$

2.6.6. Bioadhesivity test

Part of the rat skin tissue was cut and immediately secured with the mucosa side out into each glass vial *via* rubber bands and aluminum caps. Phosphate-buffered saline (PBS) was applied to vials containing rat skin tissue for 10 min. The test was carried out by gluing the skin onto the upper and lower vial bases, after which the hydrogel preparation was placed between the rat skin on the scale's left arm. The hydrogel was moistened with PBS and then attached to the skin. The vial's height was then altered to accommodate the application of hydrogel between the mucosal tissues of both vials. Once two vials were linked, the weights were held at that level. The detachment stress (dyne/cm^2) between two vials was calculated using the adhesive forces presented below [27].

$$\text{Bioadhesive strength} : \frac{m.g}{A} \tag{12}$$

where m is the weight required to remove the gel from the skin, g is the acceleration due to gravity (980 cm/s^2), and A is surface area of the exposed mucosa (cm^2).

2.6.7. Ex vivo dermatokinetic study

Dermatokinetic assays using Franz diffusion cells were carried out following the previous method [28]. Rat skins were cut and soaked in PBS pH 7.4 for 30 min before being attached to Franz diffusion cells. The medium used in this study was simulated wound fluid, which was arranged as a receiver compartment. The receiver compartment was heated to 37 ± 1 °C and agitated at 600 rpm. Parafilm® was used to close off the donor area. A 1 g sample of CPL MPs hydrogel was put into the skin using a syringe needle for 30 s, and a 5 g cylindrical weight was placed on top of the skin to keep the formula in place during the experiment.

The samples were taken at intervals of 1, 2, 3, 4, 5, 6, 8, and 24 h. After removing the hydrogel, the skin was cleansed with deionized water to remove any residue particles. The biopsy incision was 5 mm in diameter and was made in the skin. Next, the skin was transferred to a 1.5 mL Eppendorf® tube and heated in a water bath at 60 °C for 2–3 min. The epidermal layer was separated from the dermis layer using forceps. The extraction process of the drug on the skin layer was carried out by adding 1 mL of methanol separately, and each mixture was homogenized for 10 min. The sample was then centrifuged at 3000 rpm for 15 min. Supernatants were collected and then measured using UV–Vis spectrophotometer and following procedure Section 2.3.2. C_{max}, T_{max} and AUC_{0-24} were determined using PK Solver software (China Pharmaceutical University, Nanjing, China).

2.6.8. Ex vivo antibacterial activity test using infection skin model

2.6.8.1. Ex vivo test preparation on rat skin infection model. The skin was sterilized by immersing it in 70 % ethanol for 1 h. The skin was sensitized to laminar airflow (LAF) for 20 min prior to the experiment. Furthermore, the sterilized skin was administered an intradermal injection of 50 mL of BSA solution, which was equal to 0.5 McFarland. The skin piece was next positioned aseptically on a Petri plate filled with TSA media. The skin was then aseptically transferred to a new TSA Petri dish, and the Petri dish was incubated at 37 °C for 7 days.

2.6.8.2. Antibacterial activity test of ex vivo hydrogel preparations on skin infection model. The antibacterial activity of the *ex vivo* skin infection model was carried out using diffusion Franz diffusion cells [29]. In this study, rat skin of average thickness was used, and a skin infection model was placed on diffusion cells. Before the study, a dilution of CPL MPs hydrogel and CPL hydrogel was prepared by dissolving in DMSO. The skin was collected and 1.5 mL of sterile water was added to a 1.5 mL Eppendorf tube after hydrogel treatments had been left on for 6, 12, and 24 h, respectively. Next, the mixture was homogenized and TSA medium was added to a Petri dish with 20 mL of homogenous samples. The sample with the medium was incubated for 24 h at 37 °C. Additionally, the same method was used to apply both blank hydrogel and CPL hydrogel to infected skin as a control. We determined the log CFU/mL of the samples.

2.7. Analytical statistic

All data obtained for this study were reported as means of the standard deviation (SD) and computed using Microsoft Excel® 2016 (Microsoft Corporation, Redmond, USA). The data were analyzed using GraphPad Prism® version 6 (GraphPad Software, San Diego, California, USA) and the SPSS version with a significance value of $p = 0.05$.

3. Result & discussion

3.1. Particle size, zeta potential and polydispersity index (PDI) of CPL MPs

All ingredients used in the preparation of CPL MPs have been reported to be non-toxic and safe for clinical purposes [30]. As a cross-linker agent, CPL MPs were prepared by solvent evaporation and stabilized by glutaraldehyde. Moreover, glutaraldehyde has also been reported to introduce intermolecular cross-linking in proteins or to modify adsorbed proteins on amino-glutaraldehyde bonds [31]. Glutaraldehyde-mediated cross-linking of whey proteins was formed by aggregates of whey protein by whey protein intermolecular amide bonds (β-lactoglobulin (BLG) bands) and glutaraldehyde as follows the reaction in Fig. 1. This approach successfully fabricated MPs in this study by designing formulations with a variation of CPL, WPI concentration and WPI:CPL ratio. The MPs' physical characteristics were then evaluated in Table 1 and Fig. 2A.

The results show that particle sizes of CPL MPs were produced in the range of 0.56 ± 0.13 μm to 35.71 ± 5.23 μm. Conversely, samples with variation in CPL concentration show significant particle size variation between formulations. Moreover, the formulation with a variation of WPI concentration also shows significant particle size variation between formulations ($p < 0.05$) with an increase of 3.62 μm. It concludes that the concentration of WPI can produce a more compact protein structure so that the higher the protein concentration, the more it will be able to increase particle size [32]. The same trend also occurs in variations in the ratio of WPI and CPL (1:1, 2:1, 8:1, 16:1), of which a 1:1 ratio was found to yield significantly larger particle size compared to the rest ($p <$

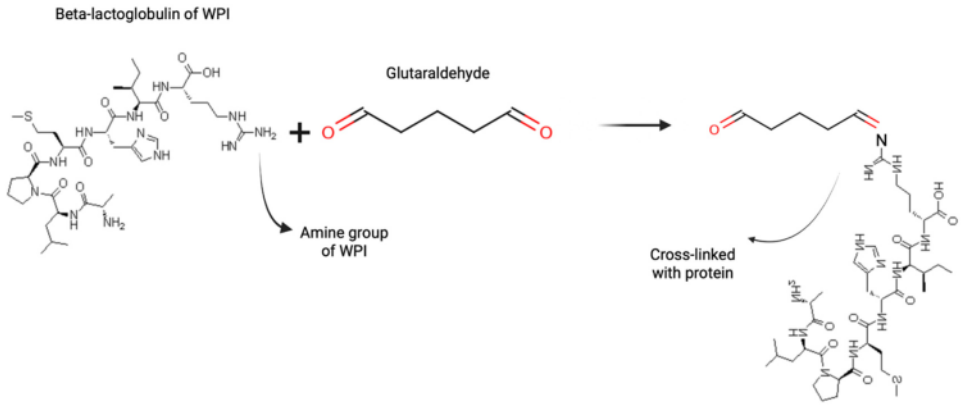

Fig. 1. The cross-linked reaction of Amine group of WPI and glutaraldehyde.

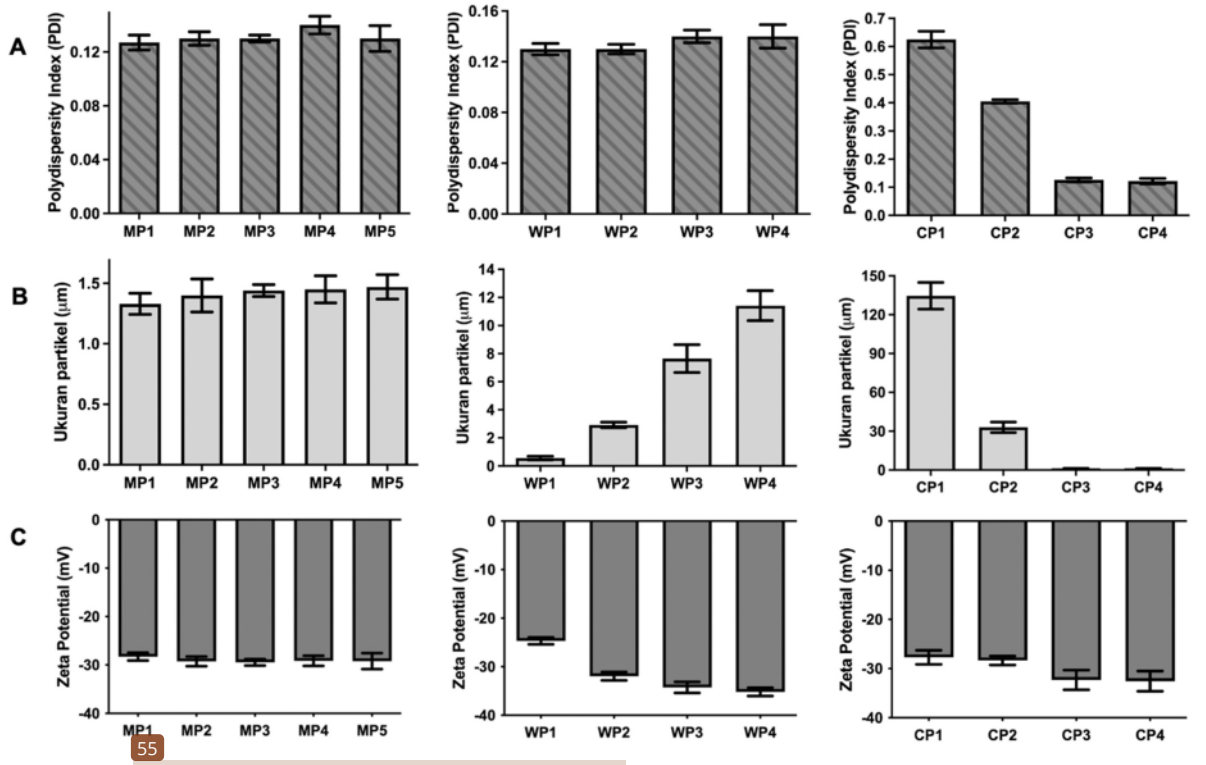

Fig. 2. Particle size (A), polydispersity index (B) and zeta potential (C) of CPL MPs prepared with whey protein (WPI) (means ± SD, $n = 3$).

0.05). This increase may be due to increased hydrophobic interactions between encapsulated and absorbed CPL in the main component of the protein isolate β-lactoglobulin with an increase in WPI concentration. Solution at pH 8.0 allows ligands to enter the hydrophobic nucleus and bind to many hydrophobic molecules, causing an increase in particle size [33]. These findings also showed that the CPL/WPI microparticle size was dependent on the ratio of WPI: CPL in the system (core: coating ratio), and that this ratio could be raised by increasing the WPI content in the formulations [34].

PDI was carried out to characterize the molecular weight of a polymer. Based on the results (Fig. 2B), samples with a variation of CPL WPI concentrations show no significant results between formulations ($p > 0.05$). While the different outcomes are noticeably seen in the ratio of WPI:CPL, the higher solution of WPI in formulation shows decreased PDI

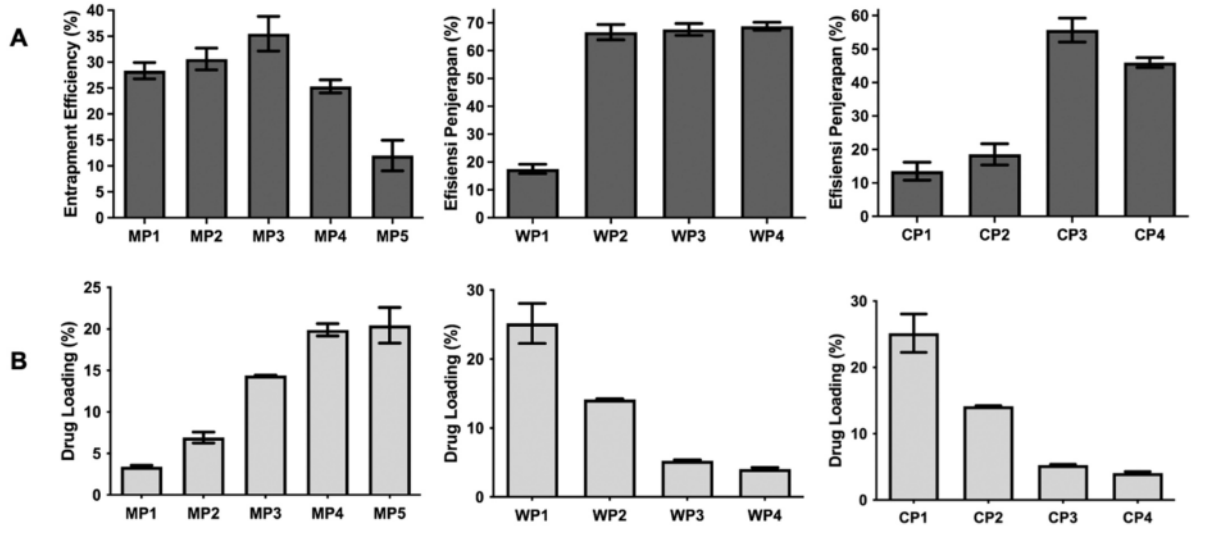

Fig. 3. EE (A) and DL of (B) diagram of CPL MPs with a variation of CPL, WPI and ratio of CPI: WPI concentration (means ± SD, $n = 3$).

value. The PDI value indicates the same trend as the particle size. PDI smaller than 0.5 is produced when the mass of WPI in WPI:CPL is within the range of 2:1 to 16:1, indicating high particle aggregation with a broad particle size distribution [30].

Measurement of zeta potential can predict the colloidal solution's stability, indicating the repulsive force between MPs. The zeta potential graphic of the CPL MPs is shown in Fig. 2C. CPL MPs have a relatively high zeta potential (*i.e.*, close to around −30 mV), indicating good stability of MPs exhibited in this study. Furthermore, increasing the concentration of CPL in the formulation has a significant effect ($p > 0.05$) on the zeta potential of MPs, indicating that the significant amount of drugs trapped in the core has no effect on the surface area of β-lactoglobulin. All formulations have extremely negative zeta potentials, which improve the physical stability of many systems by increasing the repulsive force between MPs [35]. In addition, the negative zeta potential found in this investigation may be attributable to the structure of the whey protein opening during heating at the microparticle preparation, which reveals more polar groups [36]. Furthermore, β-Lg of WPI has an isoelectric point in the range of 4.9–5.4. The second significant constituent of whey protein is α-La, with an isoelectric point of 4.6. When pH value increases above the isoelectric point, the protein produces a negative charge, which facilitates negative zeta potential. Additionally, the isoelectric point of β-Lg is in the 4.9–5.4 range. Whey protein's second important component (α-La) has an isoelectric point of 4.6. Proteins create a negative charge when the pH level rises above the isoelectric point, which supports the negative zeta potential [37,38].

3.2. EE and DL percentages

Entrapment efficiency (%EE) and drug loading (%DL) of CPL MPs are shown in Fig. 3A. CPL MPs have a higher EE value (68.78 ± 1.40 %) when the mass of WPI is in the range of 10–20 %, but there is no noticeable difference between WP2, WP3 and WP4 ($p > 0.05$). The same trend occurred in the WPI: CPL ratio (8:1 and 6:1), experiencing an increase in EE (55.67 ± 3.55 % and 45.98 ± 1.47 %). This value decreased significantly to 13.50 ± 2.67 % when the WPI:CPL ratio was 1:1. WPI has an amphiphilic structure that can self-assemble into different forms, thereby increasing drug encapsulation. However, this ability can be reduced if DL has been maximized. According to Li et al., the increased surface hydrophobicity of WPI aggregates can explain their higher CPL loading capacity [39]. Li et al. investigated whether the enhanced contact between hydrophobic groups during the chemical cross-linking procedure was causing the surface hydrophobicity of WPI to rise. They found that the more active hydrophobic patches among the generated WPI aggregates for binding to CPL accounted for their increased %EE and %DL.

Drug loading of CPL MPs increased significantly from 3.40 ± 1.68 % to 20.43 ± 2.15 % (Fig. 3B). Similar results have also been reported in utilizing α-lactalbumin-based nanoparticles to encapsulate resveratrol, in which the DL value increased significantly as drug content was increased, indicating a higher microparticle loading capacity with the addition of drugs [40]. Moreover, methanol as the solvent to dissolve CPL at higher concentrations modifies the protein solution's dielectric constant and induces the transition into aggregates [19]. Consequently, the total WPI aggregate formed depends on CPL concentration and the amount of solvent in the formulation. The DL of WPI aggregates produced in this preparation was much higher than what Zhang et al. reported for protein based-nanoparticles formulation (12.69 μg/mg nanoparticles) [42].

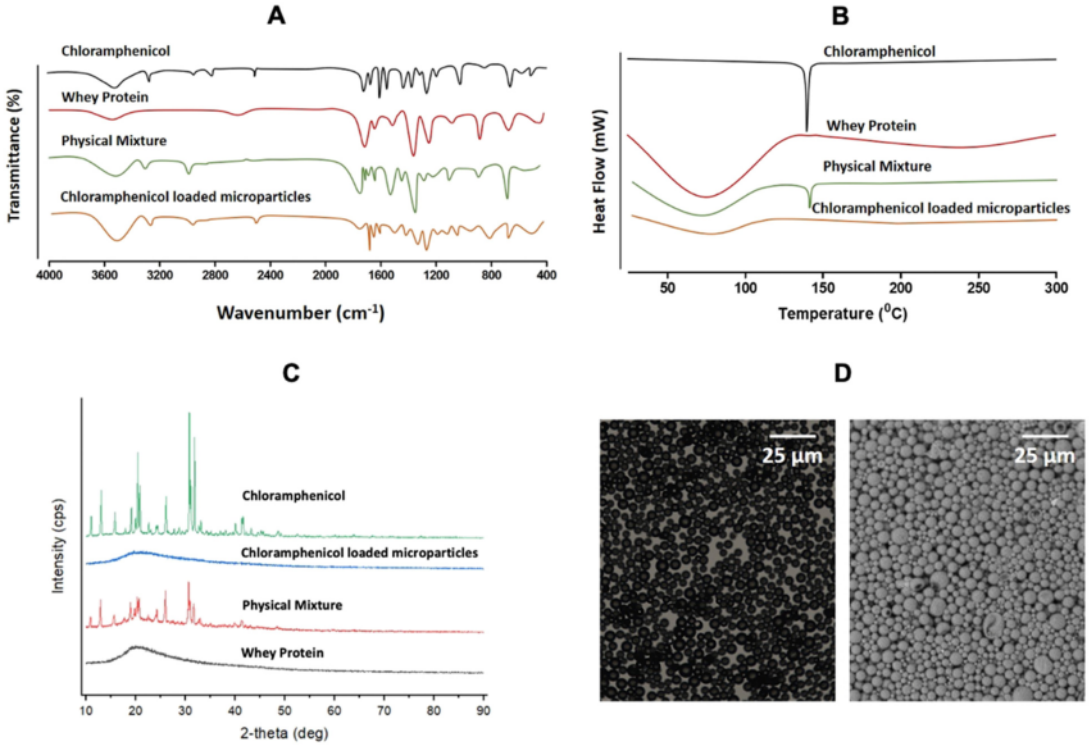

Fig. 4. FT-IR Spectra of CPL, WPI, Physical Mixture (1.5:1) and CPL MPs (A). DSC thermogram of CPL, WPI, Physical Mixture (1.5:1) and CPL MPs (B). X-ray diffractogram of CPL, WPI, Physical Mixture (1.5:1) and CPL MPs (C). SEM images of CPL-loaded MPs (D).

3.3. Powder X-ray diffraction (PXRD)

X-ray diffraction (PXRD) is essential to identify the physical state of the drug and the effect of homogenization on the crystalline structure of active substances. XRD patterns of the pure WPI, pure CPL, physical mixture (1.5:1), and CPL MPs have been compared in Fig. 4C. The sharp peaks are associated with the crystalline fraction, whereas the amorphous part is represented as broad peaks [43]. It can be observed that firm crystalline peaks are observed in CPL and physical mixture diffraction. There are two sharp dominant peaks at $2\theta = 31.82°$ and $2\theta = 26.1°$ in CPL and $2\theta = 30.64°$ and $2\theta = 25.98°$ in the physical mixture (1.5:1). Two broad peaks were also observed at around 21.5° in CPL-loaded MPs and 21.46 in WPI. The same pattern was observed previously for WPI studies [43]. However, the crystalline peaks almost disappeared in the XRD pattern of CPL MPs and WPI, indicating the disruption of the crystalline form of CPL after encapsulation and entrapment of CPL into WPI-based MPs.

3.4. Differential scanning calorimetry (DSC)

To assess the physicochemical interactions between the formulation chemicals and to ascertain whether crystallinity was preserved during the encapsulation procedure, a thermal analysis of the DSC was carried out. Thermograms of pure CPL, pure WPI, physical mixture and CPL-loaded MPs are presented in Fig. 4B. The DSC curve of pure WPI exhibits a broad endothermic peak between 40 and 120 °C, centred at 85 °C. The primary whey protein components (β-lactoglobulins and α-lactalbumin) undergo heat-induced transitions, which cause this distinctive endotherm. Similar characteristics were also seen in the physical mixture WPI:CPL (1.5:1) and in prior literature [44]. The endothermic point remained sharp at 159 °C, representing CPL's melting point and crystallinity (pure CPL and physical mixture). The endothermic point at 159 °C was not investigated in the pure WPI and CPL-loaded MPs. However, in CPL MPs, an endothermic peak was observed only in pure WPI, showing that CPL was distributed molecularly in the polymer matrix and hence properly encapsulated in WPI MPs. Endothermic peaks and melting points were identified following the encapsulation of DIM with protein nanoparticles, providing strong evidence of nanoencapsulation [45].

3.5. Fourier-transform infrared spectroscopy (FT-IR) analysis

FT-IR analysis was used to determine the functional groups and interactions between pure WPI, pure CPL, physical mixture, and CPL-loaded MPs. The results are presented in Fig. 4A. Major interesting peaks are observed in 3200–3600 cm^{-1}, indicating the presence of O—H and N—H bonds. The broad peak at around 2800–2500 cm^{-1} is also associated with O—H stretching vibration. O—H stretching was remarkably shifted after CPL was encapsulated in WPI MPs due to the interaction of CPL and WPI. These changes suggested that hydrogen bonding was formed between β-lactoglobulin and CPL. In the inset spectrum, major interesting peaks are observed in 3200–3600 cm^{-1}, indicating the presence of O—H and N—H bonds [34]. The presence of strong peaks appeared on the CPL spectrum at 3493 cm^{-1}, which is associated with O—H stretching vibration; spectrum 3218 cm^{-1} is associated with N—H stretching vibration bond; spectrum 2978 cm^{-1} is associated with aromatic C—H stretching vibration, spectrum 1668 cm^{-1} with C=O stretching vibrations; and spectrum 1561 cm^{-1} is associated with NO_2 stretching peak [46]. The entire spectrum was detected in CPL encapsulated into MPs, indicating that encapsulation had been successfully performed on the system. Amides I, II, and III are regarded as typical WPI spectra, indicating the presence of WPI's primary components β-lactoglobulin and α-lactalbumin. The amide I band mainly confirms the presence of C=O stretch vibration and N—H bending. The middle absorption band II shown correlates with the structural combination group of C—N stretch with N—H deformation, while the amide III bands are associated with C—O bending vibration [47]. Amide I in the spectrum of 1745 cm^{-1}, amide II at 1451 cm^{-1}, and amide III at 1241 cm^{-1} are present in CPL-loaded MPs and physical mixture. The C=O stretching vibration carbonyl groups are primarily responsible for the Amid I observed in the encapsulated CPL at 1600–1700 cm^{1}. The binding of CPL to β-lactoglobulin was demonstrated by comparing the WPI spectrum with the encapsulated CPL. Wang et al. reported similar outcomes [33]. The spectrum of CPL-loaded MPs shows most of the characteristic peaks identical to the spectrum of WPI and CPL, which indicates the encapsulation procedure was successfully carried out. The change in intensity indicates the hydrophobic interaction of CPL and lactoglobulin complexes. These findings align with DIM-based polymerized whey protein nanoparticles [35].

3.6. SEM analysis

Morphology of CPL-loaded microparticle formulation was observed using SEM. As shown in Fig. 4D, the CPL MPs show the spherical shape of the particles. The size of CPL MPs found in this experiment was similar to that observed in the DLS analysis (~25 μm). Particle size is closely related to drug penetration into target tissues; Fig. 3D shows that CAP MPs meet the particle size criteria to penetrate the stratum corneum lipid layer through the lipidic intercellular route or aqueous pores, which can penetrate to a depth of >2 mm efficiently into hair follicles. Another study also used the solvent evaporation method and prepared MPs, resulting in particle sizes of 6–25 μm [49]. Similar studies have also been described by previous studies [20], in which nanoparticle formulation of frankincense essential oil-loaded whey with a particle size of 321 ± 22.42 nm showed a good healing effect for skin wounds. This capability can be supported if the particle size is within the range of 10–100 nm based on confirmation by studies on human, porcine or murine skin [50]. Moreover, the permeability of MPs into the skin is influenced by the shape of the particles. A spherical shape has an excellent ability to penetrate the skin because it is symmetrical in all three dimensions; thus, it can be located deep in the epidermis and dermis layers.

3.7. *In vitro* microparticle drug release of CPL MPs

The drug release behaviour of CPL compared to CPL MPs formulation is presented in Fig. 5A. To mimic the physiological condition of the skin, *in vitro* drug release was prepared using simulated wound fluid. In this study, encapsulation of the drug into microparticle form improved the drug release profile. The drug release of CPL MPs was examined as the time in which the drugs needed to be completely soluble and migrate from the initial form as in the polymeric system to the simulated wound fluid until attained maximum drug accumulation. The experiment showed that 99.40 ± 7.01 % CPL was released from the microparticle formulation after 24 h. Meanwhile, the amount of drug release from pure CPL was around 95.43 ± 2.41 % after 6 h and then CPL reached maximum release. For simulated wound fluid, the estimated drug release during the first hour was 4.76 ± 0.16 %. After that, approximately 10.31 ± 0.23 %, 24.81 ± 1.03 %, 42.04 ± 1.21 % and 62.39 ± 1.68 % of CPL were released from MPs within 2 h, 4 h, 6 h, and 8 h, respectively. By comparing both CPL and CPL MPs, a quick release lasting up to only 6 h was observed in pure CPL, while that in CPL MP's needed 24 h to completely release, showing the contribution of particle encapsulate and the sustained released drug was achieved. The CPL MPs formulations showed sustained release patterns up to 24 h. This behaviour is related to an enlarged CPL surface area, leading to an increased drug release, with a controlled release profile [51]. Following that, a quick release lasting up to 24 h was observed; weakly bound CPL that was released and attached to the surface of the microparticle may have caused the drug release. The solubility of WPI in simulated wound fluid can be attributed to the release profile of WPL from MPs, which predicts prolonged release by causing erosion of the microparticle

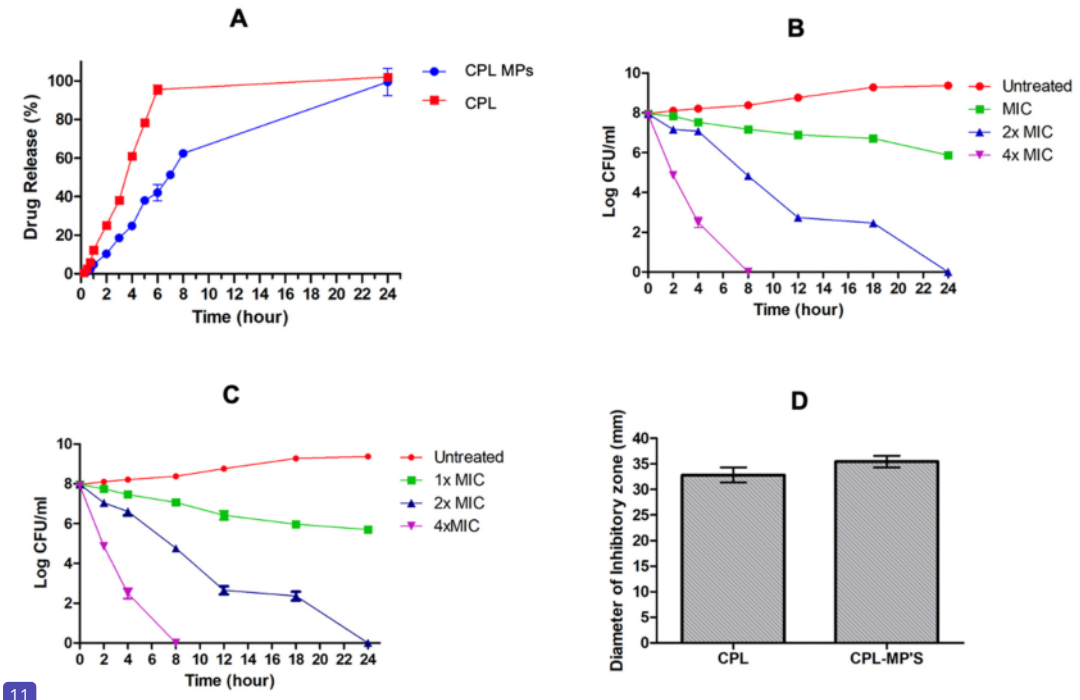

Fig. 5. *In vitro* release profiles of CPL-loaded MPs in comparison with the pure CPL (A). Time–kill assay of CPL-loaded MPs (B) and pure CPL (C) against *Staphylococcus aureus* (means ± SD, n = 3). Diameter of inhibitory zone of CPL-loaded MPs against *Staphylococcus aureus* (means ± SD, n = 3) (D).

Table 2
Kinetic modeling of pure-CPL and CPL-loaded MPs (means ± SD, *n* = 3).

Formulation	R and K value of kinetic model										
	Zero-order		First-order		Higuchi		Korsmeyer-Peppas			Hixson-Crowell	
	R	K	R	K	R	K	R	K	n	R	K
Pure CPL	0.9814	0.015	0.7495	0.000	0.7623	0.029	0.9658	0.007	0.001	0.91877	0.000
CPL MPs	0.8481	0.005	0.6279	0.000	0.8677	0.018	0.2097	0.006	0.001	0.9642	0.000

matrix.

3.8. Mathematical modeling of the kinetics of drug release

The experimental drug release was employed in multiple kinetic models to further understand the process of CPL release from MPs. The most acceptable mathematical models chosen based on the correlation coefficient value. Based on Table 2, it was concluded that the best results of CPL MPs were observed with R2 value of 0.91877. According to the results, the release behaviour of the CPL-loaded MPs formulation followed the Hixson–Crowell kinetic model. The drug release from these spherical sustained-release dosage forms depends on matrix drug diffusion and polymeric matrix erosion during polymer degradation [52]. The regular area of a collection of particles was found by Hixson and Crowell to be proportional to the volume cube root. The Hixson-Crowell cube root law describes particle release from a system where the surface area and diameter of the particles change [22]. In this work, the applicability of these equations was tested. Hixson and Crowell recognized that the rate of dissolution depends on the surface contacting with the applied solvent. Increased surface area leads to faster dissolution [21]. Because of the differences in surface area and diameter, this model corresponds well to drug release from MPs.

3.9. Determination of MIC and MBC

This work compared the bactericidal properties of pure CPL and CPL MPs. The MIC and MBC values of CPL MPs and pure CPL are 12.5 μg/mL and 25 μg/mL, respectively. The result shows that the MIC value at the lowest concentration indicates strong antibacterial activity. Next, the MBC value is determined. The MBC value was greater than the MIC value, indicating that a larger concentration of CPL was required to kill bacterial cultures. Moreover, MIC values of samples were lower than MBC values. The ratio of MBC to MIC is <4. A ratio of 4 indicates bactericidal activity, and a ratio > 4 shows bacteriostatic activity [53]. Accordingly, a higher concentration of CPL MPs was required to kill the SA. Our study also suggests that CPL should be in solution form or MPs formulation to exhibit bactericidal activity.

The results showed that the inhibition zones of pure CPL and CPL MPs were 35.45 ± 1.14 mm and 32.82 ± 1.48 mm, respectively (Fig. 6C). This might be because the substance disperses in the media, improving its capacity to penetrate the SA cell membrane. Previous research has shown that CPL prevents bacterial ribosomes from producing peptidyl transferase. The 50S ribosomal subunit's 23S rRNA contains residues A2451 and A2452, which this activity preferentially binds to [54]. CPL's ability to successfully permeate SA cell membranes may have contributed to its strong antibacterial action against SA when

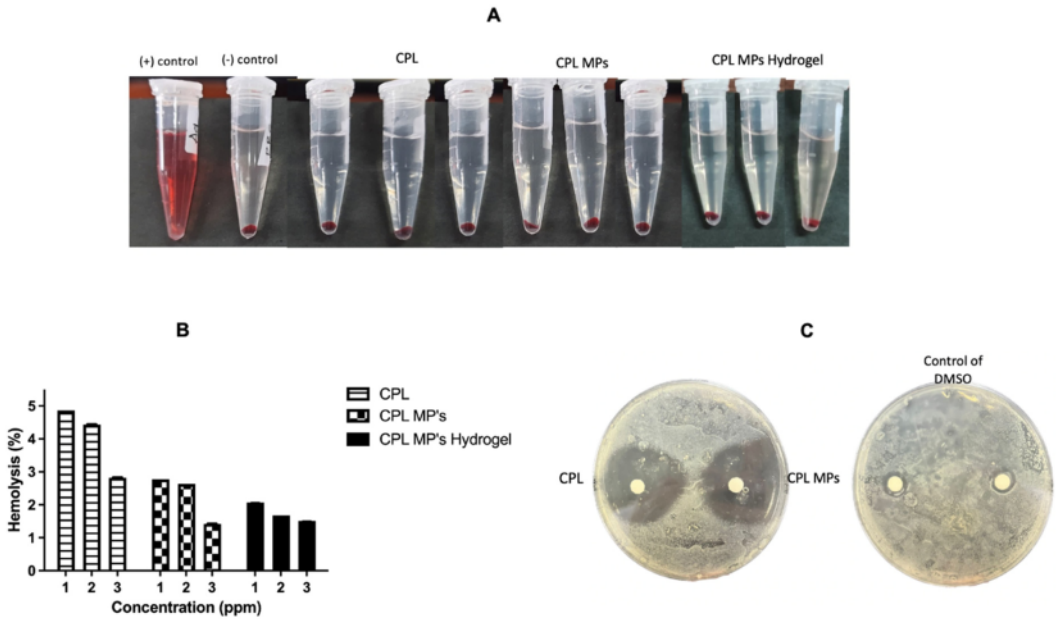

Fig. 6. Hemolysis result of CPL Mps hydrogel, CPL-loaded MPs and pure CPL with concentrations of 500, 50 and 5 μg/mL (Aquadest and PBS as positive and negative controls, respectively) (A). Hemolysis percentage of CPL-loaded MPs and pure CPL (B). Inhibitory zone of CPL-loaded MPs against *Staphylococcus aureus* compared with control (means ± SD, $n = 3$) (C).

used in solution form. Notably, our control study using DMSO alone did not show antibacterial activity. Moreover, the formulation in the form of MPs showed higher antibacterial activity compared with CPL solutions. This may be due to the increased water solubility of CPL once in the MPs, enhancing CAP's capacity to efficiently permeate SA cell membranes.

3.10. Time–kill assay

The time–kill assay was performed to examine the time required for the CPL to completely kill the SA. Time–kill curves of free CPL and CPL MPs in DMSO *versus* SA are depicted in Fig. 5B. The viable SA colony-forming unit increased by about 9.37 ± 0.05 log CFU/mL after 24 h of cultivation in the control (untreated) group. With MIC values, CPL solutions and CPL MPs were unable to kill 99.99 % of SA cultures after 24 h. When 2× MIC values were observed, no feasible SA cultures were found after 24 h in the case of either CPL solutions or CAP MPs. Furthermore, the time needed to eliminate 100 % of SA cultures was decreased to 8 h after incubation with 4× MIC values of both CPL and CPL MPs solutions. The results achieved in this work indicate that the killing rate of CPL in the microparticle-based formulation is based on how much CPL is present in the bacterial culture medium.

3.11. Hemolysis test

The cytotoxicity of chemicals on RBCs can be quickly assessed using the hemolysis test. These RBCs will burst open entirely in the presence of water, releasing their hemoglobin content. In a similar vein, changes in osmotic pressure on the surface of RBCs caused by exposure to external elements can cause significant lysis. When RBCs are damaged or lysed, they emit adenosine diphosphate, which stimulates platelet assembly on the foreign body surface, speeds up the coagulation and thrombotic cascade pathways, and disrupts the body's natural ability to heal the wound [55]. Therefore, a good wound dressing membrane should not compromise the coagulation pathway or the integrity of the circulating RBC. By spectrophotometrically lysing RBC at 540 nm, the hemolytic potential of CPL MPs and CPL MPs hydrogel was calculated. As shown in Fig. 6A–B, different concentrations of CPL MPs (5–500 μg/mL) showed hemolysis percentages in the range of 1.42–2.76 % and CPL MPs hydrogel in the range of 1.51–2.07 %, whereas pure CPL showed a higher hemolysis percentage of 2.82–4.86 %. According to the standard, materials exhibiting hemolysis > 5 % are thought to be hemolytic, those between 2 and 5 % are thought to be slightly hemolytic, and those <2 % are thought to be non-hemolytic [20]. From the results above, it can be concluded that the fabrication in the form of CPL-loaded MPs is compatible with RBCs because it consists of natural polymer.

3.12. Characteristics of hydrogel

3.12.1. pH measurement

Because the application of CPL MPs hydrogel should not irritate the skin, the pH of the formulation is very important. The pH of the hydrogel surface for each formula is in the range of 5.45 ± 0.04 to 5.55 ± 0.01, as shown in Fig. 7B, which is very close to normal skin pH of 5 to 6 [56], indicating that the formulation will be tolerated by the skin and will not interfere with the wound healing process.

3.12.2. Viscosity and rheological evaluation

Viscosity evaluation in this study used a Brookfield viscometer with spindle 7. The viscosity of CPL MPs hydrogel preparation can be seen in Fig. 7E, which shows that the viscosity of preparations obtained in this study for F1 to F5, respectively, were 2266.66 ± 230.94 cPs, 3200 ± 173.20 cPs, 6900 ± 173.21 cPs, 9433.33 ± 152.75 cPs, and 23,066.66 ± 832.67 cPs. Then, the viscosity test results from statistical analysis data showed that F1, F2 and F3 with respective chitosan concentrations of 1 % (w/w), 1.25 % (w/w) and 1.5 % (w/w) have no significantly different values ($p > 0.05$). Meanwhile, the F4–F5 formulation has a significantly different value ($p < 0.05$) from F1. The good viscosity range in gels is in the field of 2000–4000 cPs, and other studies state that the viscosity of gels can reach up to 16,000 cPs; therefore, F1, F2 and F3 are within the required viscosity range [57,58]. More importantly, chitosan

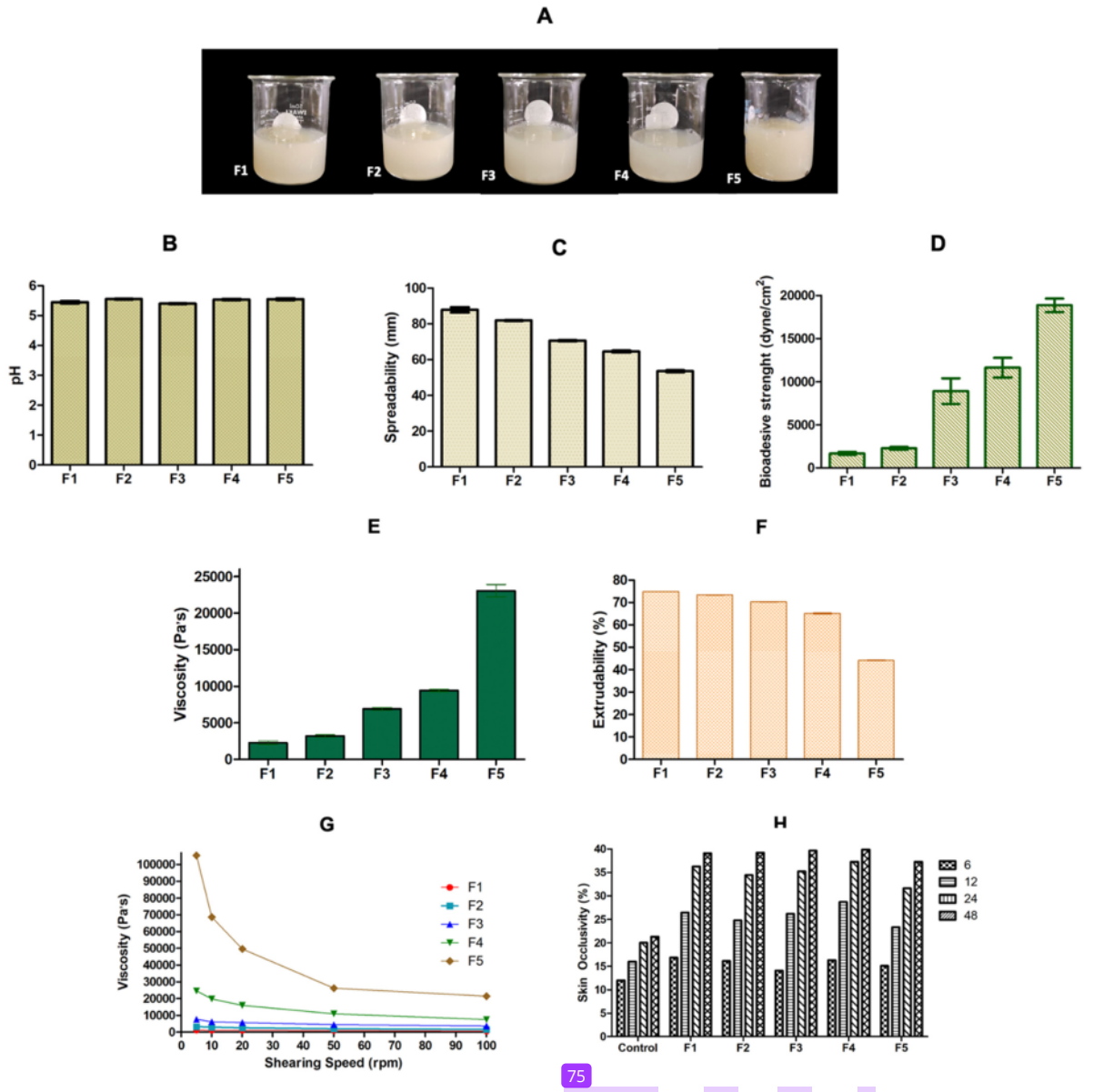

Fig. 7. Formulation of CPL MPs Hydrogel with variation concentration of chitosan (F1: 1 %; F2: 1,25 %; F3: 1,5 %; F4; 1,75 %; F5: 2 %) (A). pH (B), Spreadability (C), Bioadhesive strength (D), Viscosity (E), Extrudability (F), Rheology (G) and Skin occlusivity (H) of CPL MPs hydrogel (means ± SD, $n = 3$).

has an intrinsic viscosity of 1.2×10^5 to 3.2×10^5 Da with molecular weight (MW) in the range of 3.2 to 6.52 dL/g [59], in which the amount of chitosan concentration in the formulation can increase the value of hydrogel viscosity. Based on the results of rheological measurements (Fig. 7G), all sample flow behaviours exhibited non-Newtonian or pseudoplastic behaviour ($n < 1$). Pseudoplastic flow is a viscosity flow that continues to decrease as the rate of shear increases. Thus, it can be estimated that an Increase in spreadability will occur at higher shear speeds or after dilution with liquids [57].

3.12.3. Spreadability

Poor spreadability can cause inhomogeneous distribution of particles, which can in turn affect the amount of dose applied as well as the efficiency of the active ingredients penetrating the skin [60]. The spreadability of hydrogel preparation was determined by the hydrogel's ability to spread on the skin's surface. Good spreadability can ensure optimal distribution of hydrogel when applied to the skin. The spread test results of CPL MPs Hydrogel preparations reveal a value between 53.52 ± 0.50 mm and 87.84 ± 1.45 mm (Fig. 6C), which indicates that CPL MPs hydrogel has good spreadability. The results of the ANOVA analysis show that the spreadability of CPL MPs hydrogel is not significant between all formulations ($p > 0.05$), with the exception of F4 and F5 to F1. Spreadability is inversely proportional to viscosity [61]. Good spreadability of the preparation is in the range of 50–70 mm; therefore F3, F4 and F5 are qualifying criteria, and F3 is the most optimal formulation. The results of the measurement in Fig. 7C show that the

greater the concentration of chitosan, the smaller the spreadability of the hydrogel.

3.12.4. Skin occlusivity test

The capacity of the formulation to preserve skin moisture properties was predicted using an *in vitro* model of skin occlusivity. Over 48 h, the percentage of occlusion factors (Fig. 7H) was evaluated for each formulation (F1–F5), and a filter paper without formulation was utilized as reference. The occlusion factor values of all hydrogel formulas showed a significant difference ($p < 0.05$) compared to the control, and chitosan represented a good occlusion factor. This indicates that incorporating CPL MPs into the hydrogel can increase the occlusive value. Due to the lowering of the corneocyte slits, higher occlusion may improve skin moisture for 48 h, allowing drugs to penetrate to deeper layers of the skin [26]. According to statistical analysis, there was no difference between any CPL MPs hydrogel formulation's occlusive value ($p > 0.05$).

3.12.5. Extrudability percentage

Hydrogel extrusion from the tube is essential during application. A sufficient consistency is necessary to remove the gel from the tube because hydrogels with high consistency may not come out of the tube, while gels with low viscosity may flow too freely. The extrudability of all hydrogel formulations (F1–F5) is shown in Fig. 7F, with values of 74.9 ± 0.01 %, 73.37 ± 0.05 %, 70.3 ± 0.06 %, 65.13 ± 0.22 % and 44.17 ± 0.11 %, respectively. More than 70 % of the contents of the gel formulations F1–F3 can be extruded, demonstrating their strong extrusion capacity, with the exception of F4 and F5, where only 60 % of the contents could be extruded. Based on statistical analysis, F1 has no significant values to F2 and F3. Furthermore, F4 and F5 are significant to F1, F2 and F3. This indicates that the increased chitosan concentration affects the increasing viscosity, thereby reducing the ease of extrusion from the tube.

3.12.6. Bioadhesive test

Good bioadhesive properties can ensure a long retention time for the applied drug formulation to guarantee effective local drug concentrations and expected pharmacological responses. Bioadhesive measurements are found in Fig. 7D, which shows that the higher the concentration of chitosan used, the higher the bioadhesive strength of the preparation with F1 (1682.36 ± 171.41 dyne/cm^2), F2 (2276.13 ± 171.41 dyne/cm^2), F3 (8906.59 ± 1484.43 dyne/cm^2), F4 (11,628.05 ± 1133.75 dyne/cm^2), and F5 (18,852.29 ± 771.33 dyne/cm^2) value. The statistical analysis showed that F1 and F2, as well as F4 and F5, showed no significant value ($p > 0.05$). The increased flexibility of chitosan hydrogel of CPL MPs can improve the contact between the gel and the skin tissue, thereby encouraging the penetration of polymer chains into the tissue to form a strong bond, which leads to an increase in the strength of adhesion [62]. Thus, it also increases the effectiveness of the active substance in reaching the target. Therefore, in this test, the F3 formula was chosen as the optimum formula with a concentration of 1.5 % (w/w) that can provide good pH, dispersion, viscosity, skin occlusivity and bioadhesiveness.

3.13. Ex vivo dermatokinetic study

Ex vivo dermatokinetic study was performed on non-infected rat skin models. To investigate the kinetics of the release of CPL MPs formulation, dermatokinetic studies of the hydrogel are carried out after application to the skin. To confirm that the release of CPL occurs in the skin, the skin sample was vortexed with 2 mL of methanol at each time interval. We compared the dermatokinetic profile of this study with a hydrogel containing CPL without formulation in the form of MPs as a control to assess whether the release of drugs affects the state of drug particles. Our findings in Fig. 8A show that at 1 h and 2 h after measurements, no CPL was found in the pure-CPL hydrogel supernatant and

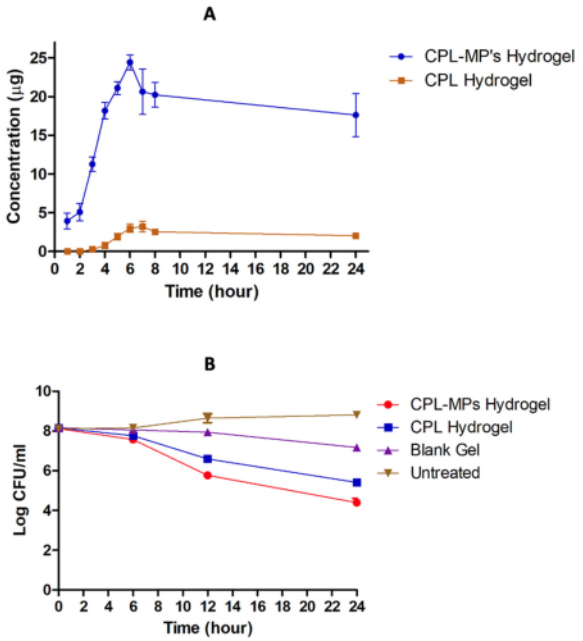

Fig. 8. Dermatokinetic tests with CPL hydrogel and CPL MPs hydrogel revealed total CPL (A) (means ± SD, n = 3). Bacterial viability (log CFU/mL) in an *ex vivo* skin infection wound model (*S. aureus*) following the administration of free CPL in the form of a hydrogel, MPs hydrogel and blank hydrogel (means ± SD, n = 3) (B).

that free CPL permeated to the receiver compartment more rapidly in contrast to CPL MPs hydrogel after 2 h. There was 2.05 ± 0.22 µg of CPL after 24 h, which indicates that the CPL without MPs formulation showed hydrophobic properties, making it difficult to penetrate the skin membrane. On the other hand, measurements at 1 h to 24 h show a CPL found in the CPL MPs hydrogel supernatant with an optimal concentration of 24.43 ± 0.95 µg at 6 h. This is in line with the main objective of this study, *i.e.*, to deliver CPL MPs to the local target of the first layer of skin, where SA colonizes, infecting the skin locally.

The concentration of CPL released from the MPs form in the skin *vs.* time of administration is depicted as the kinetic profile of hydrogel in normal skin. Table 3 shows the dermatokinetic profile of CPL MPs hydrogel and pure-CPL hydrogel after application, including C_{max}, T_{max}, $T_{1/2}$, *AUC*, and *MRT*. The results also showed that the CPL content in dermal layers obtained pure-CPL hydrogel was remarkably lower compared with that of CPL MPs hydrogel. The C_{max} (24.44 ± 0.95 g/cm^3) was reached in 6.00 h, according to the kinetic profile of CPL MPs. In comparison to CPL MPs hydrogel, the profile of pure-CPL hydrogel had a lower C_{max} (3.58 ± 0.30 g/cm^3 in 6.67 ± 0.57 h), but the differences were not statistically significant ($p > 0.05$). Additionally, the C_{max} for both the pure-CPL hydrogel and the CPL MPs hydrogel in the dermal layers was reached in the same T_{max}. The findings show that, in comparison to pure-CPL hydrogel, CPL MPs hydrogel can deliver much higher concentrations of CPL to the skin. The great *ex vivo* skin bioavailability of the microparticle method is shown by the AUC value of CPL MPs hydrogel, which was found to be substantially higher ($p < 0.05$) than that of pure-CPL hydrogel. It was discovered that the MRT value of CPL MPs hydrogel was considerably different from the pure-CPL hydrogel ($p < 0.05$) in terms of retention duration in the skin. A high MRT value can be advantageous for reducing the application time of CPL MPs hydrogels in treating skin infections associated with local infection formation [29]. This reduced application time may increase patients' acceptance of (and compliance with) this approach. Our results

Table 3
Dermatokinetic parameters of hydrogel in infected *ex vivo* skin infection models formed by SA following the application of pure-CPL Hydrogel, and CPL MPs Hydrogel (means ± SD, $n = 3$).

Condition	Formulation	C_{max} (μg/cm^3)	T_{max} (h)	$T_{1/2}$ (h)	AUC (h. μg/cm^3)	MRT (h)
Skin infection model by SA	Pure CP hydrogel	3.58 ± 0.30	6.67 ± 0.57	35.71 ± 11.99	47.51 ± 3.32	56.22 ± 16.37
	CPL MPs hydrogel	24.44 ± 0.95	6 ± 0.00	496.50 ± 749.87	417.62 ± 4.22	719.07 ± 1082.14

conclude that a responsive CPL MPs hydrogel approach can successfully deliver MPs into *ex vivo* infection models.

3.14. Ex vivo antibacterial activity test using infection skin model

To test the efficiency of CPL MPs hydrogel as an antibacterial agent, researchers used an *ex vivo* skin infection model. We sought to determine whether CPL MPs hydrogel could reduce bacterial bioburdens produced from SA by counting cells' log CFU/mL number. This test was carried out on CPL MPs hydrogel, pure-CPL hydrogel, blank hydrogel without CPL, and an untreated sample as a control. The test results are found in Fig. 8B. In *ex vivo* skin infections, the highest antibacterial activity was achieved after applying CPL MPs hydrogels compared to pure-CPL hydrogel, as measured by the reduction of bacterial bioburden after 24 h. A value of 8.22 ± 0.11 log CFU/mL to 8.81 ± 0.18 log CFU/mL increase in bacterial bioburden was seen in untreated samples, which indicates the validity of the control sample. Blank hydrogel without drugs showed a value of 8.16 ± 0.04 log CFU/mL to 7.11 ± 0.07 log CFU/mL decrease in bioburden properties. The antibacterial activity in the blank hydrogel was due to the ability of chitosan as a natural polymer to inhibit microorganisms, as explained in a previous study [18].

Analysis of *ex vivo* antibacterial activity showed an enhancement of 8.02 ± 0.10 log CFU/mL to 4.40 ± 0.20 log CFU/mL after 24 h when CPL is incorporated into MPs in hydrogel form. This indicates that chitosan hydrogel may enhance the antibacterial activity of CPL MPs. Incorporating antibacterial compounds into chitosan hydrogels has been shown to boost their antibacterial activity in some experiments [18,36,63]. Furthermore, dermatokinetic experiments demonstrated the bioavailability of CPL MPs hydrogel in *ex vivo* skin, which is why this method was successful in eliminating 99.98 % SA infections. Therefore, there are two primary benefits associated with the delivery of CPL-loaded MPs in chitosan hydrogel. First, this approach can control the dermatokinetic profile of CPL MPs. Second, this approach may improve the efficacy of CPL MPs hydrogels in *ex vivo* infection models of rat skin formed by SA compared to CPL without MPs hydrogel formulations. The encouraging findings of this study have validated the study's premise, demonstrating that CPL can be efficiently transported to the skin utilizing MPs, and then, once incorporated into the chitosan hydrogel formula, can exhibit its antimicrobial action to target infection. To improve the antibacterial efficacy of wound therapy, our delivery system's key advantage lies in its selective delivery ability to locally target as well as its long retention period in areas of infection on the skin. The combination of MPs with chitosan hydrogels can selectively be a feasible alternative to existing wound infection care, as MPs are employed for the topical administration of antimicrobial drugs to wounds.

4. Conclusion

Wound treatments using dermal delivery system are now receiving significant attention as potential for staving off infection. In this study, hydrogels are made from chitosan polymers in which the MPs of whey protein containing CPL are embedded inside the system. CPL-loaded MPs showed desired physical and encapsulation characteristics with particle sizes in the range of 0.56 ± 0.13 μm to 35.71 ± 5.23 μm and EE value of 68.78 ± 1.40 %. The drug release behaviour of CPL from CPL MPs formulation showed a value of 99.40 ± 7.01 % after 24 h, and then the cytotoxicity of MPs chemicals on RBCs can be quickly assessed using the hemolysis test. Essentially, analysis of *ex vivo* antibacterial activity showed an enhancement of 99.98 % after 24 h when CPL was incorporated into MPs in hydrogel form. Compared to pure-CPL hydrogel, the combination delivery method developed in this study has a higher residence duration in the skin, which may increase the effectiveness of antibacterial treatment in skin wound infections. It appears likely that hydrogels created using this technique can be utilized to heal wounds successfully. To further examine the efficacy of this technique, *in vivo* investigations on suitable animal models should be conducted.

Declaration of competing interest

The authors declare that they have no known competing financial interests or personal relationships that could have appeared to influence the work reported in this paper.

Data availability

Data will be made available on request.

Acknowledgement

Tri Puspita Roska expresses gratitude to Deutscher Akademischer Austausch Dienst (DAAD) for providing the scholarship. The Ministry of Education, Culture, Research, and Technology of the Republic of Indonesia also provided funding for this study under contract number 090/E5/PG.02.00/PT/2022. The authors thank Glanbia Nutritionals, Inc., Fitchburg, USA for providing whey protein (WPI).

References

[1] J.F. Guest, N. Ayoub, T. McIlwraith, I. Uchegbu, A. Gerrish, D. Weidlich, K. Vowden, P. Vowden, Health economic burden that different wound types impose on the UK's National Health Service, Int. Wound J. 14 (2017) 322–330, https://doi.org/10.1111/iwj.12603.
[2] J.E. Cefalu, K.M. Barrier, A.H. Davis, Wound infections in critical care, Crit. Care Nurs. Clin. North Am. 29 (2017) 81–96, https://doi.org/10.1016/j.cnc.2016.09.009.
[3] J.S. Boateng, K.H. Matthews, H.N.E. Stevens, G.M. Eccleston, Wound healing dressings and drug delivery systems: a review, J. Pharm. Sci. 97 (2008) 2892–2923, https://doi.org/10.1002/jps.21210.
[4] S.G. Ingebrigtsen, N. Škalko-Basnet, A.M. Holsæter, Development and optimization of a new processing approach for manufacturing topical liposomes-in-hydrogel drug formulations by dual asymmetric centrifugation, Drug Dev. Ind. Pharm. 42 (2016) 1375–1383, https://doi.org/10.3109/03639045.2015.1135940.
[5] D.A. Kuznetsova, D.R. Gabdrakhmanov, G.A. Gaynanova, L.A. Vasileva, D. M. Kuznetsov, S.S. Lukashenko, A.D. Voloshina, A.S. Sapunova, I.R. Nizameev, M. K. Kadirov, K.A. Petrov, L.Y. Zakharova, G.v. Sibgatullina, D.v. Samigullin, Novel biocompatible liposomal formulations for encapsulation of hydrophilic drugs – chloramphenicol and cisplatin, Colloids Surf A Physicochem Eng Asp. 610 (2021), https://doi.org/10.1016/j.colsurfa.2020.125673.
[6] S.I. Miller, Antibiotic resistance and regulation of the gram-negative bacterial outer membrane barrier by host innate immune molecules, MBio 7 (2016), https://doi.org/10.1128/mBio.01541-16.
[7] A.D. Permana, Q.K. Anjani, E. Sartini, F. Utomo, A.J. Volpe-Zanutto, Y.M. Paredes, S.A.Mardikasari Evary, R. Muh, I.N. Pratama, R.F.Donnelly Tuany, Selective delivery of silver nanoparticles for improved treatment of biofilm skin infection using bacteria-responsive microparticles loaded into dissolving microneedles, Mater. Sci. Eng. C 120 (2021), 111786, https://doi.org/10.1016/j.msec.2020.111786.
[8] S. Yasasvini, R.S. Anusa, B.N. VedhaHari, P.C. Prabhu, D. RamyaDevi, Topical hydrogel matrix loaded with Simvastatin microparticles for enhanced wound healing activity, Mater. Sci. Eng. C 72 (2017) 160–167, https://doi.org/10.1016/j.msec.2016.11.038.

[9] X. Delabranche, A. Berger, J. Boisramé-Helms, F. Meziani, Microparticles and infectious diseases, Med. Mal. Infect. 42 (2012) 335–343, https://doi.org/10.1016/j.medmal.2012.05.011.

[10] M. Lengyel, N. Kállai-Szabó, V. Antal, A.J. Laki, I. Antal, Microparticles, microspheres, and microcapsules for advanced drug delivery, Sci. Pharm. 87 (2019), https://doi.org/10.3390/scipharm87030020.

[11] A. George, P.A. Shah, P.S. Shrivastav, Natural biodegradable polymers based nano-formulations for drug delivery: a review, Int. J. Pharm. 561 (2019) 244–264, https://doi.org/10.1016/j.ijpharm.2019.03.011.

[12] A.R. Madureira, C.I. Pereira, A.M.P. Gomes, M.E. Pintado, F. Xavier Malcata, Bovine whey proteins – overview on their main biological properties, Food Res. Int. 40 (2007) 1197–1211, https://doi.org/10.1016/j.foodres.2007.07.005.

[13] M.A. Farooq, M. Aquib, S. Ghayas, R. Bushra, D. Haleem Khan, A. Parveen, B. Wang, Whey protein: a functional and promising material for drug delivery systems recent developments and future prospects, Polym. Adv. Technol. 30 (2019) 2183–2191, https://doi.org/10.1002/pat.4676.

[14] Z. Liu, C. Liu, X. Sun, S. Zhang, Y. Yuan, D. Wang, Y. Xu, Fabrication and characterization of cold-gelation whey protein-chitosan complex hydrogels for the controlled release of curcumin, Food Hydrocoll. 103 (2020), https://doi.org/10.1016/j.foodhyd.2019.105619.

[15] A. Aliyah, W.W. Oktaviana, K.S. Dwipayanti, A.P. Erdiana, R.N. Utami, A. D. Permana, Enhanced skin localization of doxycycline using microparticles and hydrogel: effect of oleic acid as penetration enhancer, Pharmaciana 11 (2021) 239, https://doi.org/10.12928/pharmaciana.v11i2.21044.

[16] C. Xiao, R. You, Y. Fan, Y. Zhang, Tunable functional hydrogels formed from a versatile water-soluble chitosan, Int. J. Biol. Macromol. 85 (2016) 386–390, https://doi.org/10.1016/j.ijbiomac.2016.01.006.

[17] K. Mohan, A.R. Ganesan, T. Muralisankar, R. Jayakumar, P. Sathishkumar, V. Uthayakumar, R. Chandirasekar, N. Revathi, Recent insights into the extraction, characterization, and bioactivities of chitin and chitosan from insects, Trends Food Sci. Technol. 105 (2020) 17–42, https://doi.org/10.1016/j.tifs.2020.08.016.

[18] M.E. Abd El-Hack, M.T. El-Saadony, M.E. Shafi, N.M. Zabermawi, M. Arif, G. E. Batiha, A.F. Khafaga, Y.M. Abd El-Hakim, A.A. Al-Sagheer, Antimicrobial and antioxidant properties of chitosan and its derivatives and their applications: a review, Int. J. Biol. Macromol. 164 (2020) 2726–2744, https://doi.org/10.1016/j.ijbiomac.2020.08.153.

[19] A. Jain, G. Sharma, G. Ghoshal, P. Kesharwani, B. Singh, U.S. Shivhare, O. P. Katare, Lycopene loaded whey protein isolate nanoparticles: an innovative endeavor for enhanced bioavailability of lycopene and anti-cancer activity, Int. J. Pharm. 546 (2018) 97–105, https://doi.org/10.1016/j.ijpharm.2018.04.061.

[20] M.M. Agwa, S. Sabra, N.A. Atwa, H.A. Dahdooh, R.M. Lithy, H. Elmotasem, Potential of frankincense essential oil-loaded whey protein nanoparticles embedded in frankincense resin as a wound healing film based on green technology, J. Drug Deliv. Sci. Technol. 71 (2022), 103291, https://doi.org/10.1016/j.jddst.2022.103291.

[21] C. Bradford, R. Freeman, S.L. Percival, In vitro study of sustained antimicrobial activity of a new silver alginate dressing, J. Am. Col. Certif. Wound Spec. 1 (2009) 117–120, https://doi.org/10.1016/j.jcws.2009.09.001.

[22] B.B.K. Reddy, K.E.V. Nagoji, S. Sahoo, Preparation and in vitro & in vivo evaluation of cephalexin matrix tablets, Braz. J. Pharm Sci. 54 (2018), https://doi.org/10.1590/s2175-97902018000317277.

[23] A.D. Permana, A.J. Paredes, F. Volpe-Zanutto, Q.K. Anjani, E. Utomo, R. F. Donnelly, Dissolving microneedle-mediated dermal delivery of itraconazole nanocrystals for improved treatment of cutaneous candidiasis, Eur. J. Pharm. Biopharm. 154 (2020) 50–61, https://doi.org/10.1016/j.ejpb.2020.06.025.

[24] A.D. Permana, M. Mir, E. Utomo, R.F. Donnelly, Bacterially sensitive nanoparticle-based dissolving microneedles of doxycycline for enhanced treatment of bacterial biofilm skin infection: a proof of concept study, Int. J. Pharm. X 2 (2020), 100047, https://doi.org/10.1016/j.ijpx.2020.100047.

[25] M. Mir, A.D. Permana, I.A. Tekko, H.O. McCarthy, N. Ahmed, Asim.ur Rehman, R. F. Donnelly, Microneedle liquid injection system assisted delivery of infection responsive nanoparticles: A promising approach for enhanced site-specific delivery of carvacrol against polymicrobial biofilms-infected wounds, Int. J. Pharm. 587 (2020) 119643, https://doi.org/10.1016/j.ijpharm.2020.119643.

[26] A.D. Permana, R.N. Utami, A.J. Courtenay, M.A. Manggau, R.F. Donnelly, L. Rahman, Phytosomal nanocarriers as platforms for improved delivery of natural antioxidant and photoprotective compounds in propolis: an approach for enhanced both dissolution behaviour in biorelevant media and skin retention profiles, J. Photochem. Photobiol. B 205 (2020), 111846, https://doi.org/10.1016/j.jphotobiol.2020.111846.

[27] U.C. Galgatte, A.B. Kumbhar, P.D. Chaudhari, Development of in situ gel for nasal delivery: design, optimization, in vitro and in vivo evaluation, Drug Deliv. 21 (2014) 62–73, https://doi.org/10.3109/10717544.2013.849778.

[28] A.D. Permana, I.A. Tekko, M.T.C. McCrudden, Q.K. Anjani, D. Ramadon, H. O. McCarthy, R.F. Donnelly, Solid lipid nanoparticle-based dissolving microneedles: a promising intradermal lymph targeting drug delivery system with potential for enhanced treatment of lymphatic filariasis, J. Control Release 316 (2019) 34–52, https://doi.org/10.1016/j.jconrel.2019.10.004.

[29] A.D. Permana, R.N. Utami, P. Layadi, A. Himawan, N. Juniarti, Q.K. Anjani, E. Utomo, S.A. Mardikasari, A. Arjuna, R.F. Donnelly, Thermosensitive and mucoadhesive in situ ocular gel for effective local delivery and antifungal activity of itraconazole nanocrystal in the treatment of fungal keratitis, Int. J. Pharm. 602 (2021), 120623, https://doi.org/10.1016/j.ijpharm.2021.120623.

[30] Q. Liu, Y. Sun, J. Cheng, M. Guo, Development of whey protein nanoparticles as carriers to deliver soy isoflavones, LWT Food Sci. Technol. 155 (2022), 112953, https://doi.org/10.1016/j.lwt.2021.112953.

[31] L. Betancor, F. López-Gallego, A. Hidalgo, N. Alonso-Morales, G.D.-O.C. Mateo, R. Fernández-Lafuente, J.M. Guisán, Different mechanisms of protein immobilization on glutaraldehyde activated supports: effect of support activation and immobilization conditions, Enzym. Microb. Technol. 39 (2006) 877–882, https://doi.org/10.1016/j.enzmictec.2006.01.014.

[32] C. le Bourvellec, C.M.G.C. Renard, Interactions between polyphenols and macromolecules: quantification methods and mechanisms, Crit. Rev. Food Sci. Nutr. 52 (2012) 213–248, https://doi.org/10.1080/10408398.2010.499808.

[33] C. Wang, X. Zhou, H. Wang, X. Sun, M. Guo, Interactions between β-lactoglobulin and 3,3′-diindolylmethane in model system, Molecules 24 (2019) 2151, https://doi.org/10.3390/molecules24112151.

[34] A. Abbasi, Z. Emam-Djomeh, M.A.E. Mousavi, D. Davoodi, Stability of vitamin D3 encapsulated in nanoparticles of whey protein isolate, Food Chem. 143 (2014) 379–383, https://doi.org/10.1016/j.foodchem.2013.08.018.

[35] A. Khan, C. Wang, X. Sun, A. Killpartrick, M. Guo, Preparation and characterization of whey protein Isolate–DIM nanoparticles, Int. J. Mol. Sci. 20 (2019) 3917, https://doi.org/10.3390/ijms20163917.

[36] W. Zhang, J. Chen, Y. Chen, W. Xia, Y.L. Xiong, H. Wang, Enhanced physicochemical properties of chitosan/whey protein isolate composite film by sodium laurate-modified TiO2 nanoparticles, Carbohydr. Polym. 138 (2016) 59–65, https://doi.org/10.1016/j.carbpol.2015.11.031.

[37] B. Vardhanabhuti, M.A. Kelly, P.J. Luck, M.A. Drake, E.A. Foegeding, Roles of charge interactions on astringency of whey proteins at low pH, J. Dairy Sci. 93 (2010) 1890–1899, https://doi.org/10.3168/jds.2009-2780.

[38] I. Evdokimov, L. Alieva, V. Varlamov, V. Kurchenko, V.-. Haritonov, T. Butkevich, Usage of chitosan in dairy products production, Food Raw Mat. 3 (2015) 29–39, https://doi.org/10.12737/13117.

[39] M. Li, Y. Ma, M.O. Ngadi, Binding of curcumin to β-lactoglobulin and its effect on antioxidant characteristics of curcumin, Food Chem. 141 (2013) 1504–1511, https://doi.org/10.1016/j.foodchem.2013.02.099.

[40] Y. Liu, L. Gao, J. Yi, Y. Fan, X. Wu, Y. Zhang, α-lactalbumin and chitosan core–shell nanoparticles: resveratrol loading, protection, and antioxidant activity, Food Funct. 11 (2020) 1525–1536, https://doi.org/10.1039/C9FO01998G.

[42] Y. Zhang, M. Zhao, Z. Ning, S. Yu, N. Tang, F. Zhou, Development of a sono-assembled, bifunctional soy peptide nanoparticle for cellular delivery of hydrophobic active cargoes, J. Agric. Food Chem. 66 (2018) 4208–4218, https://doi.org/10.1021/acs.jafc.7b05889.

[43] R.V.de B. Fernandes, S.V. Borges, D.A. Botrel, C.R. de Oliveira, Physical and chemical properties of encapsulated rosemary essential oil by spray drying using whey protein-inulin blends as carriers, Int. J. Food Sci. Technol. 49 (2014) 1522–1529, https://doi.org/10.1111/ijfs.12449.

[44] X. Shen, C. Zhao, J. Lu, M. Guo, Physicochemical properties of whey-protein-stabilized astaxanthin nanodispersion and its transport via a Caco-2 monolayer, J. Agric. Food Chem. 66 (2018) 1472–1478, https://doi.org/10.1021/acs.jafc.7b05284.

[45] Y. Luo, Z. Teng, Q. Wang, Development of zein nanoparticles coated with carboxymethyl chitosan for encapsulation and controlled release of vitamin D3, J. Agric. Food Chem. 60 (2012) 836–843, https://doi.org/10.1021/jf204194z.

[46] Z. Teng, Y. Luo, Q. Wang, Carboxymethyl chitosan–soy protein complex nanoparticles for the encapsulation and controlled release of vitamin D3, Food Chem. 141 (2013) 524–532, https://doi.org/10.1016/j.foodchem.2013.03.043.

[47] A. Goyal, V. Sharma, M.K. Sihag, S.K. Tomar, S. Arora, L. Sabikhi, A.K. Singh, Development and physico-chemical characterization of microencapsulated flaxseed oil powder: a functional ingredient for omega-3 fortification, Powder Technol. 286 (2015) 527–537, https://doi.org/10.1016/j.powtec.2015.08.050.

[49] C.A. Busatto, M.E. Taverna, M.R. Lescano, C. Zalazar, D.A. Estenoz, Preparation and characterization of lignin microparticles-in-alginate beads for atrazine controlled release, J. Polym. Environ. 27 (2019) 2831–2841, https://doi.org/10.1007/s10924-019-01564-2.

[50] M. Schneider, F. Stracke, S. Hansen, U.F. Schaefer, Nanoparticles and their interactions with the dermal barrier, Dermatoendocrinol 1 (2009) 197–206, https://doi.org/10.4161/derm.1.4.9501.

[51] P.-E. Lee, W.-S. Choo, Characterization of flaxseed oil emulsions, J. Food Sci. Technol. 52 (2015) 4378–4386, https://doi.org/10.1007/s13197-014-1495-3.

[52] N. Kamaly, B. Yameen, J. Wu, O.C. Farokhzad, Degradable controlled-release polymers and polymeric nanoparticles: mechanisms of controlling drug release, Chem. Rev. 116 (2016) 2602–2663, https://doi.org/10.1021/acs.chemrev.5b00346.

[53] M. Tato, Y. López, M.I. Morosini, A. Moreno-Bofarull, F. Garcia-Alonso, D. Gargallo-Viola, J. Vila, R. Cantón, Characterization of variables that may influence ozenoxacin in susceptibility testing, including MIC and MBC values, Diagn. Microbiol. Infect. Dis. 78 (2014) 263–267, https://doi.org/10.1016/j.diagmicrobio.2013.11.010.

[54] M. Abdollahi, S. Mostafalou, Chloramphenicol, in: Encyclopedia of Toxicology, Elsevier, 2014, pp. 837–840, https://doi.org/10.1016/B978-0-12-386454-3.00709-0.

[55] W. Yuan, Y. Feng, H. Wang, D. Yang, B. An, W. Zhang, M. Khan, J. Guo, Hemocompatible surface of electrospun nanofibrous scaffolds by ATRP modification, Mater. Sci. Eng. C 33 (2013) 3644–3651, https://doi.org/10.1016/j.msec.2013.04.048.

[56] Ó.L. Ramos, J.C. Fernandes, S.I. Silva, M.E. Pintado, F.X. Malcata, Edible films and coatings from whey proteins: a review on formulation, and on mechanical and bioactive properties, Crit. Rev. Food Sci. Nutr. 52 (2012) 533–552, https://doi.org/10.1080/10408398.2010.500528.

[57] M.M. Ibrahim, S.A. Hafez, M.M. Mahdy, Organogels, hydrogels and bigels as transdermal delivery systems for diltiazem hydrochloride, AsianJ. Pharm. Sci. 8 (2013) 48–57, https://doi.org/10.1016/j.ajps.2013.07.006.
[58] N. Harish, P. Prabhu, R. Charyulu, M. Gulzar, E.V.S. Subrahmanyam, Formulation and evaluation of in situ gels containing clotrimazole for oral candidiasis, Indian J. Pharm. Sci. 71 (2009) 421, https://doi.org/10.4103/0250-474X.57291.
[59] D.P. Chattopadhyay, M.S. Inamdar, Aqueous behaviour of chitosan, Int. J. Polym. Sci. 2010 (2010) 1–7, https://doi.org/10.1155/2010/939536.
[60] L. Montenegro, L. Rapisarda, C. Ministeri, G. Puglisi, Effects of lipids and emulsifiers on the physicochemical and sensory properties of cosmetic emulsions containing vitamin E, Cosmetics 2 (2015) 35–47, https://doi.org/10.3390/cosmetics2010035.
[61] D.R. Kryscio, P.M. Sathe, R. Lionberger, L. Yu, M.A. Bell, M. Jay, J.Z. Hilt, Spreadability measurements to assess structural equivalence (Q3) of topical Formulations—A technical note, AAPS PharmSciTech 9 (2008) 84–86, https://doi.org/10.1208/s12249-007-9009-5.
[62] X. Zhang, Y. Jiang, L. Han, X. Lu, Biodegradable polymer hydrogel-based tissue adhesives: a review, Biosurf. Biotribol. 7 (2021) 163–179, https://doi.org/10.1049/bsb2.12016.
[63] M.O. Ilomuanya, N.v. Enwuru, E. Adenokun, A. Fatunmbi, A. Adeluola, C.I. Igwilo, Title: chitosan-based microparticle encapsulated Acinetobacter baumannii phage cocktail in hydrogel matrix for the management of multidrug resistant chronic wound infection, Turk. J. Pharm. Sci. 0 (2021) 0, https://doi.org/10.4274/tjps.galenos.2021.72547.

A.Dian Permana-5_Usulan.pdf

ORIGINALITY REPORT

21%	12%	19%	2%
SIMILARITY INDEX	INTERNET SOURCES	PUBLICATIONS	STUDENT PAPERS

PRIMARY SOURCES

1	Ardiyah Nurul Fitri Marzaman, Sartini, Mukarram Mudjahid, Tri Puspita Roska, Anwar Sam, Andi Dian Permana. "Development of chloramphenicol whey protein-based microparticles incorporated into thermoresponsive in situ hydrogels for improved wound healing treatment", International Journal of Pharmaceutics, 2022 Publication	2%
2	www.mdpi.com Internet Source	2%
3	Andi Dian Permana, Alejandro J. Paredes, Fabiana Volpe-Zanutto, Qonita Kurnia Anjani, Emilia Utomo, Ryan F. Donnelly. "Dissolving microneedle-mediated dermal delivery of itraconazole nanocrystals for improved treatment of cutaneous candidiasis", European Journal of Pharmaceutics and Biopharmaceutics, 2020 Publication	1%

4	Andi Dian Permana, Qonita Kurnia Anjani, Sartini, Emilia Utomo et al. "Selective delivery of silver nanoparticles for improved treatment of biofilm skin infection using bacteria-responsive microparticles loaded into dissolving microneedles", Materials Science and Engineering: C, 2021 Publication	1 %
5	Mona M. Agwa, Sally Sabra, Nagwa A. Atwa, Heba A. Dahdooh, Rasha M. Lithy, Heba Elmotasem. "Potential of frankincense essential oil-loaded whey protein nanoparticles embedded in frankincense resin as a wound healing film based on green technology", Journal of Drug Delivery Science and Technology, 2022 Publication	1 %
6	pure.ulster.ac.uk Internet Source	1 %
7	Maria Mir, Andi Dian Permana, Ismaiel A. Tekko, Helen O. McCarthy, Naveed Ahmed, Asim. ur. Rehman, Ryan F. Donnelly. "Microneedle liquid injection system assisted delivery of infection responsive nanoparticles: A promising approach for enhanced site-specific delivery of carvacrol against polymicrobial biofilms-infected wounds", International Journal of Pharmaceutics, 2020	1 %

Publication

8	doi.org Internet Source	1 %
9	Andi Dian Permana, Maria Mir, Emilia Utomo, Ryan F. Donnelly. "Bacterially sensitive nanoparticle-based dissolving microneedles of doxycycline for enhanced treatment of bacterial biofilm skin infection: A proof of concept study", International Journal of Pharmaceutics: X, 2020 Publication	1 %
10	Qingguan Liu, Yuxue Sun, Jianjun Cheng, Mingruo Guo. "Development of whey protein nanoparticles as carriers to deliver soy isoflavones", LWT, 2022 Publication	1 %
11	Sulistiawati, Kadek Saka Dwipayanti, Muhammad Azhar, Latifah Rahman, Ermina Pakki, Achmad Himawan, Andi Dian Permana. "Enhanced skin localization of metronidazole using solid lipid microparticles incorporated into polymeric hydrogels for potential improved of rosacea treatment: An ex vivo proof of concept investigation", International Journal of Pharmaceutics, 2022 Publication	1 %
12	curis.ku.dk Internet Source	<1 %

13	www.frontiersin.org Internet Source	<1%
14	mdpi-res.com Internet Source	<1%
15	Latifah Rahman, Reni Sriyani Lembang, Subehan Lallo, Sri Resky Handayani, Usmanengsi, Andi Dian Permana. "Bioadhesive dermal patch as promising approach for improved antibacterial activity of bioactive compound of Zingiber cassumunar Roxb in ex vivo Staphylococcus aureus skin infection model", Journal of Drug Delivery Science and Technology, 2021 Publication	<1%
16	link.springer.com Internet Source	<1%
17	Andi Dian Permana, Ismaiel A. Tekko, Maelíosa T.C. McCrudden, Qonita Kurnia Anjani et al. "Solid lipid nanoparticle-based dissolving microneedles: A promising intradermal lymph targeting drug delivery system with potential for enhanced treatment of lymphatic filariasis", Journal of Controlled Release, 2019 Publication	<1%
18	Anna Lisik, Witold Musiał. "Conductomeric Evaluation of the Release Kinetics of Active	<1%

Substances from Pharmaceutical Preparations Containing Iron Ions", Materials, 2019
Publication

19	www.tandfonline.com Internet Source	<1 %
20	Carolina Oliveira Marinho, Thomás Corrêa Vianna, Ricardo Rodrigo Ramos Cecci, Luís Marangoni Júnior et al. "Effect of water kefir grain biomass on chitosan film properties", Materials Today Communications, 2022 Publication	<1 %
21	www.jfas.info Internet Source	<1 %
22	dokumen.pub Internet Source	<1 %
23	Montenegro, Lucia, Lucia Rapisarda, Carmen Ministeri, and Giovanni Puglisi. "Effects of Lipids and Emulsifiers on the Physicochemical and Sensory Properties of Cosmetic Emulsions Containing Vitamin E", Cosmetics, 2015. Publication	<1 %
24	micro.fish.hokudai.ac.jp Internet Source	<1 %
25	www.researchgate.net Internet Source	<1 %

26	N. Gnanou Besse. "Effect of various environmental parameters on the recovery of sublethally salt-damaged and acid-damaged Listeria monocytogenes", Journal of Applied Microbiology, 12/2000 Publication	<1 %
27	Pereira, Antonio G.B., André R. Fajardo, Samara Nocchi, Celso V. Nakamura, Adley F. Rubira, and Edvani C. Muniz. "Starch-based microspheres for sustained-release of curcumin: Preparation and cytotoxic effect on tumor cells", Carbohydrate Polymers, 2013. Publication	<1 %
28	coek.info Internet Source	<1 %
29	Flora Farrokhi, Mohammad Reza Ehsani, Fojan Badii, Maryam Hashemi. "Structural and thermal properties of nanofibrillated whey protein isolate in the glassy state", LWT, 2018 Publication	<1 %
30	Ashay Jain, Gajanand Sharma, Gargi Ghoshal, Prashant Kesharwani, Bhupinder Singh, U.S. Shivhare, O.P. Katare. "Lycopene loaded whey protein isolate nanoparticles: An innovative endeavor for enhanced bioavailability of lycopene and anti-cancer activity", International Journal of Pharmaceutics, 2018 Publication	<1 %

31	Mahmood Alizadeh-Sani, Arezou Khezerlou, Ali Ehsani. "Fabrication and characterization of the bionanocomposite film based on whey protein biopolymer loaded with TiO 2 nanoparticles, cellulose nanofibers and rosemary essential oil", Industrial Crops and Products, 2018 Publication	<1 %
32	Colin Bradford, Richard Freeman, Steven L. Percival. "In Vitro Study of Sustained Antimicrobial Activity of a New Silver Alginate Dressing", The Journal of the American College of Certified Wound Specialists, 2009 Publication	<1 %
33	Guidini, C.Z.. "@b-Galactosidase of Aspergillus oryzae immobilized in an ion exchange resin combining the ionic-binding and crosslinking methods: Kinetics and stability during the hydrolysis of lactose", Journal of Molecular Catalysis. B, Enzymatic, 201109 Publication	<1 %
34	knepublishing.com Internet Source	<1 %
35	researchrepository.murdoch.edu.au Internet Source	<1 %
36	Ke Peng, Lalitkumar K. Vora, Ismaiel A. Tekko, Andi Dian Permana et al. "Dissolving	<1 %

microneedle patches loaded with amphotericin B microparticles for localised and sustained intradermal delivery: Potential for enhanced treatment of cutaneous fungal infections", Journal of Controlled Release, 2021
Publication

---

37 Katayoun Morteza-Semnani, Majid Saeedi, Jafar Akbari, Shakiba Hedayati et al. "Green formulation, characterization, antifungal and biological safety evaluation of terbinafine HCl niosomes and niosomal gels manufactured by eco-friendly green method", Journal of Biomaterials Science, Polymer Edition, 2022 <1 %
Publication

---

38 Małgorzata Stanisz, Łukasz Klapiszewski, Dariusz Moszyński, Beata J. Stanisz, Teofil Jesionowski. "Evaluation of cilazapril release profiles with the use of lignin-based spherical particles", Journal of Drug Delivery Science and Technology, 2022 <1 %
Publication

---

39 Meenakshi Choudhary, Priyanka Chhabra, Amit Tyagi, Harpal Singh. "Scar free healing of full thickness diabetic wounds: A unique combination of silver nanoparticles as antimicrobial agent, calcium alginate nanoparticles as hemostatic agent, fresh <1 %

blood as nutrient/growth factor supplier and chitosan as base matrix", International Journal of Biological Macromolecules, 2021
Publication

40	Na Ji, Yan Hong, Zhengbiao Gu, Li Cheng, Zhaofeng Li, Caiming Li. "Chitosan coating of zein-carboxymethylated short-chain amylose nanocomposites improves oral bioavailability of insulin in vitro and in vivo", Journal of Controlled Release, 2019 Publication	<1 %
41	eventscribe.com Internet Source	<1 %
42	jcbr.goums.ac.ir Internet Source	<1 %
43	publikationen.bibliothek.kit.edu Internet Source	<1 %
44	www.ncbi.nlm.nih.gov Internet Source	<1 %
45	Cindy Kristina Enggi, Hansel Tridatmojo Isa, Sulistiawati Sulistiawati, Komang Agus Rai Ardika et al. "Development of thermosensitive and mucoadhesive gels of cabotegravir for enhanced permeation and retention profiles in vaginal tissue: A proof of concept study", International Journal of Pharmaceutics, 2021 Publication	<1 %

46	Submitted to Hosei University Student Paper	<1 %
47	Submitted to International Medical University Student Paper	<1 %
48	Luxiang Gao, Xiaoyu Xu, Wenxiu Liu, Jinjuan Xie, Hongyan Zhang, Shuyuan Du. "A sensitive multimode dot-filtration strip for the detection of Salmonella typhimurium using MoS2@Fe3O4", Microchimica Acta, 2022 Publication	<1 %
49	cora.ucc.ie Internet Source	<1 %
50	mail.scialert.net Internet Source	<1 %
51	Darya A. Kuznetsova, Dinar R. Gabdrakhmanov, Gulnara A. Gaynanova, Leysan A. Vasileva et al. "Novel biocompatible liposomal formulations for encapsulation of hydrophilic drugs – Chloramphenicol and cisplatin", Colloids and Surfaces A: Physicochemical and Engineering Aspects, 2021 Publication	<1 %
52	Filipa A. Vicente, Matej Huš, Blaž Likozar, Uroš Novak. " Chitin Deacetylation Using Deep Eutectic Solvents: -Supported Process	<1 %

Optimization ", ACS Sustainable Chemistry & Engineering, 2021
Publication

53	M.-H. Coconnier-Polter, V. Lievin-Le Moal, A. L. Servin. "A Lactobacillus acidophilus Strain of Human Gastrointestinal Microbiota Origin Elicits Killing of Enterovirulent Salmonella enterica Serovar Typhimurium by Triggering Lethal Bacterial Membrane Damage", Applied and Environmental Microbiology, 2005 Publication	<1 %
54	Ravit Edelman, Shira Engelberg, Lulu Fahoum, Esther G. Meyron-Holtz, Yoav D. Livney. "Potato protein- based carriers for enhancing bioavailability of astaxanthin", Food Hydrocolloids, 2019 Publication	<1 %
55	innovareacademics.in Internet Source	<1 %
56	moam.info Internet Source	<1 %
57	dspace.uib.es Internet Source	<1 %
58	eprints.uad.ac.id Internet Source	<1 %
59	faculty.uml.edu Internet Source	<1 %

60	gacetasanitaria.org Internet Source	<1%
61	www.coursehero.com Internet Source	<1%
62	www.thno.org Internet Source	<1%
63	Agata Niemczyk, Miroslawa El Fray, Steve E. Franklin. "Friction behaviour of hydrophilic lubricious coatings for medical device applications", Tribology International, 2015 Publication	<1%
64	Chen, Siqin, Gongjie Yu, Bo Zhang, Yinsong Wang, Ning Zhang, and Yan Chen. "Human serum albumin (HSA) coated liposomal indocyanine green for in vivo tumor imaging", RSC Advances, 2016. Publication	<1%
65	Jie Ouyang, Shujin Pu, Juzheng Wang, Yuefeng Deng, Chengli Yang, Sidra Naseer, Dali Li. "Enzymatic hydrolysate of geniposide directly acts as cross-linking agent for enzyme immobilization", Process Biochemistry, 2020 Publication	<1%
66	Labouta, Hagar I., and Marc Schneider. "Interaction of inorganic nanoparticles with the skin barrier: current status and critical	<1%

review", Nanomedicine Nanotechnology Biology and Medicine, 2013.
Publication

---

67 Rebecca Ann Bader. "A study of diffusion in poly(ethyleneglycol)-gelatin based semi-interpenetrating networks for use in wound healing", Polymer Bulletin, 03/2009 <1%
Publication

---

68 Sara Demartis, Qonita Kurnia Anjani, Fabiana Volpe-Zanutto, Alejandro J. Paredes et al. "Trilayer dissolving polymeric microneedle array loading Rose Bengal transfersomes as a novel adjuvant in early-stage cutaneous melanoma management", International Journal of Pharmaceutics, 2022 <1%
Publication

---

69 Tokle, T.. "Physicochemical properties of lactoferrin stabilized oil-in-water emulsions: Effects of pH, salt and heating", Food Hydrocolloids, 201107 <1%
Publication

---

70 Xinchen Du, Yujie Liu, Hongyu Yan, Muhammad Rafique, Shilin Li, Xilu Shan, Le Wu, Mingqiang Qiao, Deling Kong, Lianyong Wang. "Anti-Infective and Pro-Coagulant Chitosan-Based Hydrogel Tissue Adhesive for Sutureless Wound Closure", Biomacromolecules, 2020 <1%
Publication

71	d2caqqgqlj5e2n.cloudfront.net Internet Source	<1 %
72	doktori.bibl.u-szeged.hu Internet Source	<1 %
73	ethesis.nitrkl.ac.in Internet Source	<1 %
74	repository.wit.ie Internet Source	<1 %
75	sure.sunderland.ac.uk Internet Source	<1 %
76	unsworks.unsw.edu.au Internet Source	<1 %
77	www.dovepress.com Internet Source	<1 %
78	www.jmaterenvironsci.com Internet Source	<1 %
79	9dok.org Internet Source	<1 %
80	Chao Chang, Taoran Wang, Qiaobin Hu, Mingyong Zhou, Jingyi Xue, Yangchao Luo. "Pectin coating improves physicochemical properties of caseinate/zein nanoparticles as oral delivery vehicles for curcumin", Food Hydrocolloids, 2017 Publication	<1 %

81	Muhammad Asim Farooq, Md Aquib, Sana Ghayas, Rabia Bushra, Daulat Haleem Khan, Amna Parveen, Bo Wang. "Whey protein: A functional and promising material for drug delivery systems recent developments and future prospects", Polymers for Advanced Technologies, 2019 Publication	<1 %
82	Qingguan Liu, Yuxue Sun, Qiang Cui, Jianjun Cheng, A. Killpartrik, Alyssa H. Kemp, Mingruo Guo. "Characterization, antioxidant capacity, and bioaccessibility of Coenzyme Q10 loaded whey protein nanoparticles", LWT, 2022 Publication	<1 %
83	S Yasasvini, RS Anusa, BN VedhaHari, PC Prabhu, D RamyaDevi. "Topical hydrogel matrix loaded with Simvastatin microparticles for enhanced wound healing activity", Materials Science and Engineering: C, 2017 Publication	<1 %
84	Thunnalin Winuprasith, Piyachai Khomein, Wiphada Mitbumrung, Manop Suphantharika, Anadi Nitithamyong, David Julian McClements. "Encapsulation of vitamin D 3 in pickering emulsions stabilized by nanofibrillated mangosteen cellulose: Impact on in vitro digestion and bioaccessibility", Food Hydrocolloids, 2018 Publication	<1 %

85	Win Yee Lim, Eric Wei Chiang Chan, Chia Wei Phan, Chen Wai Wong. "Emulsion formulated using Hibiscus tiliaceus L. extract and flaxseed oil for topical application", Industrial Crops and Products, 2022 Publication	<1 %
86	Ye, Aiqian, Tao Zheng, Jack Z. Ye, and Harjinder Singh. "Potential role of the binding of whey proteins to human buccal cells on the perception of astringency in whey protein beverages", Physiology & Behavior, 2012. Publication	<1 %
87	Zhuzhu Liu, Chengzhen Liu, Xun Sun, Shuaizhong Zhang, Yongkai Yuan, Dongfeng Wang, Ying Xu. "Fabrication and characterization of cold-gelation whey protein-chitosan complex hydrogels for the controlled release of curcumin", Food Hydrocolloids, 2020 Publication	<1 %
88	academic.oup.com Internet Source	<1 %
89	bmccomplementmedtherapies.biomedcentral.com Internet Source	<1 %
90	digital.library.unt.edu Internet Source	<1 %

91	ir-library.egerton.ac.ke Internet Source	<1 %
92	jjbs.hu.edu.jo Internet Source	<1 %
93	oamjms.eu Internet Source	<1 %
94	storage.googleapis.com Internet Source	<1 %
95	www.annexpublishers.co Internet Source	<1 %
96	www.collectionscanada.gc.ca Internet Source	<1 %
97	www.science.gov Internet Source	<1 %
98	Alexandra D. Voloshina, Syumbelya K. Gumerova, Anastasiia S. Sapunova, Natalia V. Kulik et al. "The structure – Activity correlation in the family of dicationic imidazolium surfactants: Antimicrobial properties and cytotoxic effect", Biochimica et Biophysica Acta (BBA) - General Subjects, 2020 Publication	<1 %
99	Nazila Kamaly, Basit Yameen, Jun Wu, Omid C. Farokhzad. "Degradable Controlled-Release Polymers and Polymeric Nanoparticles:	<1 %

Mechanisms of Controlling Drug Release", Chemical Reviews, 2016

Publication

Exclude quotes	On	Exclude matches	< 5 words
Exclude bibliography	On		